SEGREGATION ICE FRACTURING OF RIVER BANK ROCK:

IMPLICATIONS FOR THE WIDTH OF BEDROCK CHANNELS

A thesis submitted to the faculty of
San Francisco State University
In partial fulfillment of
the requirements for
the Degree

Master of Science

In

Geosciences

Larry L. Alden

San Francisco, California

May 2015

CERTIFICATION OF APPROVAL

I certify that I have read SEGREGATION ICE FRACTURING OF RIVER BANK ROCK: IMPLICATGIONS FOR THE WIDTH OF BEDROCK CHANNELS by Larry L. Alden, that in my opinion this work meets the criteria for approving a thesis submitted in partial fulfillment of the requirement for the degree Master of Science in Geosciences at San Francisco State University.

Leonard S. Sklar, Professor of Geology

Joseph A. Barranco, Assoc. Professor of Physics and Astronomy

Jason Gurdak, Asst. Professor of Geology

SEGREGATION ICE FRACTURING OF RIVERBANK ROCK:

IMPLICATIONS FOR THE WIDTH OF BEDROCK CHANNELS

Larry L. Alden

San Francisco, California

2015

Rivers cut vertically and laterally into bedrock. However, control on the width of bedrock rivers is an unsolved problem. In alpine settings, frost cracking is one of the mechanisms that break down bedrock. Segregation ice drives growth of ice lenses within rock masses. When the temperature of the rock is within the "frost cracking window" of -3 to -8 °C, ice lenses can attract liquid water. Expanding ice lenses can exert sufficient pressure to fracture the rock. We hypothesize that alpine rivers may promote segregation ice growth at the river margin by supplying water, but also may inhibit frost cracking by supplying heat. We find support for this hypothesis in data collected along the Tuolumne and Mokelumne rivers in the Sierra Nevada, California. A 1D heat flow model predicts that frost cracking should occur above 2325 masl in this area. To test for a river effect, I measured fracture density along the Tuolumne River at ~2600 masl, finding that density at the river margin is significantly greater than on adjacent hillslopes in the Cathedral Peak granodiorite. We then deployed data loggers on the Mokelumne River (at 2490 masl) over the winter of 2013/2014 to record water, surface and subsurface rock temperatures at varying depths and distances from the river. Temperatures within the frost cracking window were only recorded at a distance of ~5 m from the river, suggesting an insulating effect from the river and snow cover. Rock temperature ~1 m deep equilibrated at ~ 2 °C. This result requires subsurface heat flow into the model space. Ongoing work includes terrestrial LiDAR scans to detect erosion of the river bank at the Mokelumne site, and further development of a 2D heat flow model to predict subsurface rock temperatures for varying surface boundary conditions and channel morphology. We expect that further analysis will reveal systematic relationships between the surface boundary conditions and rock temperature at depth, enabling predictive modeling of frost cracking intensity at the river margin.

I certify that this abstract is a correct representation of this thesis.

_______________________________ 5/14/15

Leonard S. Sklar, Professor of Geology Date

ACKNOWLEDGEMENTS

Thanks to Dr. David Dawdy and Dr. Ray Pestrong for the grants that funded the instrumentation for the NFM site

Thanks to Mr. Skye Corbett and US Geological Survey for the LiDAR scan

Thanks to the intrepid crew that assisted with the epic installation at the North Fork Mokelumne River, Alpine County, California:

Christopher Olsen

Omid Arabnia

Ryan Ford

Mike Marquez

TABLE OF CONTENTS

TABLES

FIGURES

APPENDICES

1.0 INTRODUCTION

Bedrock rivers are a primary agent for the removal of mass from the landscape. Although they occupy only a small proportion of the land surface, bedrock rivers control denudation through sediment transport. Bedrock channels set the base level for hillslopes in uplifting landscapes (Whipple et al., 2012). Channel width is an important control on channel morphology because it determines the area of sediment transport and the distribution of fluid stresses (Finnegan et al., 2007). Channel width scales with both drainage area (Montgomery and Gran, 2001) and discharge (Wobus et al, 2006). It also adjusts to tectonic forcing, carrying a signal of uplift rates (Duvall et al., 2004). However, controls on bedrock channel width are poorly understood (Finnegan et al., 2007).

Bedrock channel width generally scales with drainage area in the same manner as alluvial channels, except in some cases of highly resistant rock (Whipple, 2004). In resistant rock, channels can be narrower due to the concentration of fluid stress on vertical incision (Montgomery and Gran, 2001). Much has been learned about controls on vertical incision. Processes such as plucking, abrasion, and hydration fracturing have been shown to be important (Whipple, 2004). Channel widening is controlled by lateral incision. Do the same processes that control vertical incision also control lateral incision, or are the river banks essentially hillslopes where erosion is controlled by hillslope processes? In alpine regions one such process is frost cracking by segregation ice (Hales and Roering, 2009). Segregation ice forms in cracks and pore space in rock masses. Ice lenses grow by attracting liquid water from unfrozen zones and exert sufficient force to crack rock. Two necessary conditions for the formation of segregation ice are temperature in the range of -3 to -8 °C ("frost cracking window") (Fig. 1) and the availability of liquid water (Hales and Roering, 2007). Is frost cracking a mechanism for lateral erosion of bedrock river banks in alpine regions, and, therefore, an influence on channel width? This question has not previously been asked.

What aspects of alpine rivers might promote or inhibit frost cracking? The two main factors for segregation ice are temperature within the frost cracking window and water. Hence, the river might suppress frost cracking by supplying heat, but could also promote frost cracking by supplying liquid water. Given the temperature dependence of frost cracking, I hypothesize that there is a threshold elevation below which frost cracking does not occur. Above this threshold, the river warmth may be most influential, suppressing frost cracking in the river bed even though it may occur on the adjacent banks. I also hypothesize that there can be an elevation above which frost cracking cannot occur during the coldest season due to the lack of liquid water. Within this elevation range the river may either promote or suppress frost cracking.

In my study, I address these knowledge gaps and explore these hypotheses in the central Sierra Nevada (Fig. 2). I use climate data to identify the threshold elevation in this portion of the range and determine the sensitivity of days spent within the frost cracking window to elevation. I look for evidence in the field that fracture patterns differ between river banks and adjacent hillslopes in a manner that could be diagnostic of frost cracking. I conduct a detailed study of an eroding bedrock bank to determine how temperatures vary within the rock, seeking evidence of the influence of the river.

Finally, I develop a 2D finite element heat flow model to explore the boundary conditions needed to produce the temperature profile within the rock. Taken together these efforts are intended to determine if frost cracking of bedrock banks could matter and whether further investigation is warranted.

2.0 SEGREGATION ICE

The theory of segregation ice growth is derived from the fundamental physics of the molecular forces which attract water molecules to a substrate and thermodynamic free energy relationships (Gilpin, 1980). These forces attract liquid water to frozen zones in soil and rock, resulting in the expansion of ice lenses. The term "segregation" is used because, within a certain temperature range, a nanometer-scale film of liquid water segregates the ice and the rock. It is important to note that the theory is not based on the volumetric expansion of ice due to change of phase. Rather the theory is based on the ability of ice near a reservoir of liquid water to expand by attracting water to the frozen zone.

Segregation ice growth has been modeled as a mechanism for fracturing rock (Walder and Hallet, 1985). Laboratory experiments have detected acoustic emissions which have been placed in liquid water at sustained temperatures below 0 °C. These emissions are interpreted as evidence of expanding cracks in pore space and pre-existing microcracks of rock samples (Hallet et al., 1991). The distribution of the data (Fig. 1) from these experiments, which were conducted with various rock types, establishes that the frost cracking is most intense in the range of -3 to -8 °C. This definition of the frost cracking window has continued to be in prevailing use in recent geomorphology literature concerning segregation ice (Anderson et al., 2012; Sanders et al., 2012; Scherier, 2014).

Hales and Roering (2007) developed a temperature model to explore climatic controls on frost cracking in bedrock alpine landscapes. The model is based on a solution of the differential equation for heat conduction in one dimension.

$$T(z,t) = MAT + Tae^{-z\sqrt{\pi/(\alpha P)}}\sin[\frac{2\pi t}{P} - z\sqrt{\frac{\pi}{\alpha P}}] \quad (1)$$

In this equation temperature (*T*) depends on both the time of year (*t*) and the depth below the surface (*z*). Of the four model parameters, two can be calibrated with local temperature measurements, mean annual temperature (*MAT*) and the annual amplitude of sinusoidal variation (*Ta*). The thermal diffusivity of rock (α) will vary with lithology, and the period of the sinusoid (*P*) is 365 days.

The application of the model assumes that segregation ice growth is most robust within the frost cracking window (Hallet et al., 1991) and that liquid water is available through snowmelt and groundwater. The model can be used to estimate the duration and depth of frost cracking for given values of the climatic parameters *MAT* and *Ta*. Because elevation is a significant control on *MAT* (Lundquist and Cayan, 2007), the model can also be used to predict the elevation ranges where frost cracking should be most intense. A literature review showed that the predictions of the model are consistent with the elevations of maximum talus production in studies of rockfall (Hales and Roering, 2007). They performed their own field study in the Southern Alps, New

Zealand (Hales and Roering, 2009), confirming that the elevations of maximum talus production from alpine cliffs coincide with the predictions of the modeling. Their work supports the hypothesis that segregation ice growth is an important process on alpine hillslopes.

Other studies add additional insight into segregation ice. Murton et al. (2006) conducted experiments with lithified chalk. Using a heat flow model coupled with the fracture model of Walder and Hallet (1985), the authors were able to show that the fractures in the experiments were caused by segregation ice rather than a freeze/thaw cycle. Murton et al. (2006) also found that the fracture patterns in the experiments were similar to field observations of surficial fractures in rock embedded in permafrost. Anderson et al. (2012) studied regolith production due to frost cracking. An innovation of this study was the introduction of a penalty for the distance water must travel to reach the frost cracking zone. The penalty took the form of an exponential decay term into a model similar to equation (1). The effect of the penalty was to move the nexus of frost cracking to a greater depth in a non-permafrost case (MAT = 4 °C), but to shallower depth in a permafrost case (MAT = -3 °C). Matsuoka (2007) did long-term (1994-2006) observations of rockwall erosion due to frost cracking in the southeastern Swiss Alps. Two important findings of this study are that lack of short-term variability in near surface rock temperature correlates with snow cover and that intensive frost cracking prevails in proximity to streams and lakes. Sanders et al. (2012) focused on the crevasse that characteristically separates the moving ice at the head of an alpine glacier from the ice which adheres to the headwall. Temperature measurements from within crevasses at north facing headwalls indicated favorable conditions for segregation ice along the headwall. Thus, segregation ice is implicated as a possible mechanism for headwall retreat.

3.0 RESEARCH QUESTIONS AND HYPOTHESES

My study is focused on the question of whether segregation ice growth contributes to the breakdown of bedrock river banks in alpine regions. I hypothesize that alpine rivers may support segregation ice growth at the river margin by supplying water, but may also inhibit frost cracking by supplying heat. These hypotheses raise subsidiary questions. Where in alpine regions can frost cracking be expected to be an important process? What types of field evidence might indicate the occurrence of frost cracking? Does the alpine climate induce rock temperatures within the frost cracking window?

I chose the central Sierra Nevada for the study due its proximity to San Francisco and relative ease of access to its alpine landscapes. In particular, I have explored the alpine reaches of the Mokelumne, Stanislaus, Tuolumne, and Merced watersheds (Fig. 2). The project has four distinct, but related, elements. (1) To determine the elevation range of greatest frost cracking intensity, I used equation (1) to determine the number of days that can be expected in the frost cracking window for a given elevation, calculating the climatic parameters with data from multi-year temperature records. (2) Seeking evidence of frost cracking at the river margin, I conducted a field survey along the Tuolumne River in Yosemite National Park (Fig. 2). (3) Over the winter of

2013/2014, I deployed temperature data loggers in a bedrock bank of the North Fork Mokelumne River ("NFM") in the Highland Lakes area, Alpine County, California (Fig. 2). In combination with water and atmospheric temperature loggers, the data from this installation enables me to evaluate how the temperatures within the rock respond to the microclimate at this location. (4) Using Matlab 2012a (©Mathworks, Inc.), I developed a 2D heatflow model to analyze how the heat flow in a cross section of NFM channel responds to varying surface boundary conditions. The parameters of the model are informed by the NFM data and then generalized to model varying channel morphology and variations in boundary conditions. These distinct efforts are linked and taken together they provide insight into the role of rivers in the frost cracking of bedrock banks.

Because of the distinct nature of each of these elements, I have organized the thesis by the topic of each element. Each section is self-contained with its own subsections covering the motivation and questions, methods, results, and implications for the study. I then synthesize the insights gleaned from these four sub-projects in the discussion section. Finally, I conclude with a summary and description of ongoing work.

4.0 THE ELEVATION RANGE FOR THE LIKELY OCCURRENCE OF SEGREGATION ICE

In this subproject, I address the question of the elevation range for the occurrence of frost cracking in the central Sierra Nevada (Fig. 2). Frost cracking intensity is measured by determining the number of days spent in the frost cracking window through solutions to equation (1). The elevation information is imbedded in *MAT,* which is shown to correlate with elevation. The elevation range derived in the subproject defines the alpine region which is subject to frost cracking in the central Sierra Nevada, informing the selection of field study sites.

In the concluding subsection 4.3, equation (1) is used to predict frost cracking intensity, measured by time spent in the frost cracking window at elevation increments of 250 m. The calculations are done for the rock surface and at depths of 60, 120, and 180 cm. Note that the maximum depth for calculations in the modeling is influenced by the limitation of the sensor installation at the NFM study site (Section 6). The deepest temperature records established at that site are at ~100 cm.

4.1 Methods

I used temperature data derived from the California Data Exchange Center ("CDEC," www.cdec.ca.gov) to determine the elevation-based *MAT* profile for the central Sierra Nevada (Table I), which for this study is defined by the contiguous watersheds of the Mokelumne, Stanislaus, Tuolumne, and Merced river systems (Fig. 2). In addition, I use this data to explore the relationship of *Ta* and elevation in this region and determine the appropriate value(s) of *Ta* for use in equation (1). Equation (1) is then used to predict the elevation range for segregation ice growth by calculating the number of days spent in the frost cracking window by elevation and depth below the rock surface.

Using the robust search features of the CDEC site, I identified the reporting stations which track mean daily temperatures within the four watersheds. To minimize the impact of year-to-year variation, I excluded stations with temperature records spanning less than five years. The duration of the covered period varies from five to twenty-six years. I took the time series of the temperature records and determined *MAT* by calculating the mean of the series.

Ta was determined for selected stations by fitting a sinusoid to superimposed, multi-year temperature plots derived from the average daily temperature record described above. The best fit was determined by selecting the amplitude of the sinusoid which resulted in the least root mean square value ("RMS") for the difference between the sinusoidal prediction and the recorded temperatures for each day of the year. In the curve fitting, I only used data from days with recorded temperatures < 0 °C because *Ta* in equation (1) is an indicator of the speed with which temperatures pass through the frost cracking window.

4.2 Results

MAT decreases with elevation in the study area by ~6.16 $°\mathrm{Ckm}^{-1}$. *MAT* by elevation and station ID is summarized in Table I. Linear regressions of *MAT* verses elevation were performed for each drainage area (Appendix A). The R^2 values for the regressions range from 0.84 to 0.97. The parameters (slope and intercept) of the fit equations were compared pairwise for statistical significance at a 95% confidence level. None of the differences among the parameters was found to be statistically significant. See Appendix A for the details of the statistical testing. Hence, I use a regional linear regression (Fig. 3) to determine the *MAT* by elevation in the modeling.

$$MAT = 19.7 - 0.00616 * Elevation\ (masl) \qquad (2)$$

Because equation (1) contains a sinusoidal term, I estimate *Ta* by fitting a sinusoid to superimposed multi-year plots of daily average temperatures (Fig. 4). The best fit was determined by selecting the sinusoid that minimized the RMS for days of the year with subzero temperatures. The amplitudes that minimize the RMS values during the cold season were 8.7 °C at elevation 1024 masl and 8.4 °C at elevation 2652 masl. This method indicates a lack of correlation of *Ta* with elevation. I generated a larger sample of *Ta* estimates by comparing the 2.7% and 97.5% quartiles for *MAT* from a sample of stations across a wide range of elevations. This method also indicates that there is no correlation of *Ta* with elevation, R^2=0.058 (Fig. 5).

4.3 Modeling

Equation (1) plots as a sinusoidal surface which converges on a plane at depth (Fig.6). As the exponential decay term in equation (1) approaches zero, the temperature solution converges on *MAT*. Note that the vertical axis in Figures 6 and 7 is temperature (°C). The horizontal axes are day of the year (day 1 = first day of spring) and depth below the rock surface (cm). For the modeling to determine the threshold elevation of segregation ice growth, I use equation (2) to determine *MAT* and set *Ta* = 8.5 °C. Thermal diffusivity is set at 1 mm^2s^{-1} for all elevations. This value is the approximate midpoint between values reported for granitic and volcanic rock (Drury, 1987). To determine the duration of time spent in the frost cracking window, I solve equation (1) with set values of MAT (corresponding to fixed elevations by equation (2)) for time at elevation intervals of 250 m. The reader is directed to Figure 7 for sample plots of these solutions.

In the region of the study (Fig. 1), the model predicts that there is no time within the frost cracking window when at or below elevation 2200 masl. The first occurrence of surface temperatures within the frost cracking window is at elevation ~2200 masl (Fig. 8). At this elevation the duration of the frost cracking window is brief (< 10 days near the surface). The duration of the frost cracking window increases rapidly with increasing elevation. At NFM (elevation 2490 m.) the duration of the frost cracking window is ~60 days at the surface and ~21 days at a depth of 40 cm (Fig. 7a). As elevation increases, the duration and depth of frost cracking increase until the internal rock temperatures fall below the lower bound of the frost cracking window, first at the surface (Fig. 7b) and gradually at depth (Fig. 7c).

I solved equation (1) for number of days spent in the frost cracking window using Ta = 8.5 °C and *MAT* calculated with equation (2) for elevations beginning at 2250 masl and 250 m intervals thereafter (Fig. 8). Solutions were developed for temperatures at the surface and at depths of 60, 120, and 180 cm. The model shows that the minimum elevation in the study area for frost cracking is ~2325 masl (Fig. 8). The highest peaks in the study area are < 4000 masl. Hence, all elevations above the minimum in the central Sierra are potential zones for frost cracking.

5.0 THE FIELD STUDY ALONG THE TUOLUMNE RIVER, YOSEMITE NATIONAL PARK

My objective in this portion of the study was to seek field evidence of the influence of the river on the occurrence of frost cracking. During the summer and autumn of 2012, I conducted reconnaissance on high elevation segments of the North

Fork and Middle Fork Stanislaus, Silver Fork American, and Tuolumne Rivers (Fig. 2). I selected the Tuolumne River downstream from Tuolumne Meadows for a detailed study due to its elevation (~2600 masl) and excellent bedrock bank exposures in three members of the Tuolumne Intrusive Suite ("TIS") (Appendix B). The downstream sequence of these exposures is Cathedral Peak granodiorite ("Kcp"), the equiangular facies of the Halfdome granodiorite ("Khd"), and the tonalite of Glen Aulin ("Kga") (Fig. 9).

The hypothesis for this subproject is that, if the river promotes frost cracking at a location by supplying water, there could be observable differences between river bank rock and adjacent hillslopes in the same geologic unit. In the predominantly granitic rock of the study area (Fig. 9), any difference between the river bank and the hillslopes might be manifest in the pattern of jointing.

5.1 Methods

I conducted traverses along the Tuolumne River in the study area (Figs. 2, 9) and on adjacent hillslopes. The traverse began where the river exits the alluvial section of Tuolumne Meadows and begins to cut into Kcp at elevation 2610 masl. I concluded in an outcrop of metasedimentary rock near Glen Aulin at elevation 2400 masl (Fig. 9). Hence, the entire traverse is within the elevation range for frost cracking as predicted by the modeling of subsection 4.3. We made observations of regional joint patterns in each member of the TIS exposed on this traverse. We also noted any observed variations on those patterns at the river margin. Key observations were documented in field notes and photographs.

I measured joints and fractures in each member of TIS (Fig. 9) in the study area. The measurements consisted of joint spacing, orientation, aperture (width of joint), length, continuity, and aspect (facing direction of an outcrop) at the location of each set of measurements. Length and spacing measurements were made with a 30 m tape. Orientation and aspect were measured with a Brunton compass. Where significant variation of jointing at the river margin and adjacent hillslopes were observed, measurements were taken both at the river margin and on nearby outcrops in the same unit. Differences in measurements of joint spacing at the river bank and nearby outcrops in the same unit were analyzed to determine whether such differences are statistically significant .

5.2 Results

The predominant regional joint pattern in Kcp in the study area is surface parallel sheet jointing (Fig. 10). The regional joint patterns in the Khd and Kga units are steeply dipping to vertical, trending approximately normal to the Tuolumne River (Fig. 11). Joint spacing is generally decimeter to meter scale. These joints are continuous from hillslopes to the river margin. I did not observe systematic differences between the joint patterns at the river margin and adjacent hillslopes in the outer members of the TIS along this traverse. Hence, the jointing in these units did not display a clearly identifiable signal of frost cracking.

However, in the Kcp unit there are numerous outcrops along the river margin with surface parallel joints that were much more closely spaced than those on nearby outcrops just a few meters distant from the river. Such outcrops were observed on both banks of the river. Hence, aspect is not a differentiating factor in the jointing. The clear difference in jointing between river bank and hillslope was unique to Kcp for this traverse. We made sample measurements of the vertical separation of these joints (Table II).

The joint spacing of the river bank and non-river bank outcrops have been statistically analyzed (Appendix C). The mean spacing in the Kcp river banks was 7.3 cm. The mean spacing in outcrops at distances ranging from 2.5 to 8.5 m from the river was 28.6 cm. The difference of 21.3 cm is significant at a > 99% confidence level (Appendix C). The results of this analysis show that the difference between the groups of outcrops is significant with a high degree of confidence.

<u>5.3 Interpretations</u>

The greater joint density at the river margin in the Kcp unit suggests two possible interpretations. First, that there is a mechanical weathering process that occurs at the river bank and not in outcrops even a few meters away from the active channel (Table II). Alternatively, if the same process occurs everywhere in the landscape, it occurs with greater intensity at the river margin. A possible explanation for the influence of the river is that it provides a reservoir of liquid water when the landscape is within the frost cracking window. This finding motivates the temperature profile study at the NFM site.

6.0 THE NFM TEMPERATURE STUDY

In this portion of the study I seek to determine the temperature response of a bedrock river bank that is within the elevation range for frost cracking (Section 4) in the central Sierra Nevada study area. To find an appropriate site, I performed reconnaissance on high elevation bedrock segments in the Tuolumne, Stanislaus, and Mokelumne watersheds (Fig. 2) during the summers of 2012 and 2013. The NFM site was selected due to relative ease of access from Highland Lakes Road in Alpine County, California and the fact that it is not located in a designating wilderness area, which brings restrictions on activity. The site is also located in an area without maintained foot trails, ~0.7 km from the nearest vehicle access point, reducing the likelihood of vandalism. The elevation of the site is 2490 masl, and there is bedrock bank composed of massive andesite.

The lithology is the Relief Peak formation, an extensive Miocene volcanic field. The primary rock type per the unit description on the USGS 15 minute Markleeville quadrangle is undivided andesite and basalt flows (Armin et al., 1984). At the study site there is a bedrock bank of extrusive rock. The opposite bank is alluvial. The lower portion of the bedrock bank is a ramp sloping ~15° toward the thalweg (Fig. 12). Numerous angular clasts with intermediate axis length of 2 to 16 cm are present on the ramp. The ramp intersects a subvertical cliff ~4.5 m from the low flow channel (Fig. 12). The aspect of the cliff is 045°. The cliff face is highly fractured in irregular patterns on a scale that is consistent with the size of the clasts on the ramp. The color of the rock on the cliff varies from reddish brown to the dark color typical of andesite. The reddish brown hue can also be seen on many of the clasts on the ramp, but not on the bedrock ramp surface. Where the ramp and cliff meet, there is a notch undercutting the cliff face (Fig. 12a). The overhead view shows the curvature of the river Fig. 12b). It appears likely that during spring food, the river discharge is pushed up against the base of the cliff, focusing fluid stress and causing erosion by clast abrasion.

6.1 Deployment of temperature sensors

I deployed four thermistors in the rock, two in the ramp and two in horizontal holes drilled into the cliff at depths ranging from 31 to 95 cm (Figs. 13, 14). The void space was filled by inserting pipe insulation and filling the uppermost few cm of each hole with sprayed foam insulation. The surface of each hole was sealed with Sikaflex caulking. In addition, we installed one thermistor in the river and one on the rock surface near the base of the cliff (Fig. 14). A seventh data logger for recording atmospheric temperature was tied to a tree at a height that we judged to be above the likely maximum snow depth. All seven data loggers were programmed to record temperatures hourly. I used Hobo STMB series temperature sensors at positions 1, 2, 4, and in the river (Fig. 14). These sensors have a measurement range of -40 to 100 °C, total accuracy of < ± 0.2 °C, and resolution of < ± 0.03 °C. These four sensors were connected to a Hobo H21 microstation data logger. The sensors at position 3 and on the rock surface were connected to a two-channel Hobo U23 data logger which has a measurement range of -40 to 70 °C, an accuracy of ± 0.21 °C, and a resolution of ± 0.02 °C. I used a Hobo U22 data logger to record atmospheric temperature. The measurement specifications of this unit are identical with the U23 unit. The U23 and

Microstation data loggers were installed in an outdoor electric box (Fig. 13d). The installation was complete on September 30, 2013.

Hourly snow depth was downloaded from the CDEC for the Ebbetts Pass weather station. The station is located approximately 6 km from the NFM study site at elevation 2670 masl (Fig. 2). This station is maintained by the Natural Resources Conservation Service ("NRCS"), a division of the United States Department of Agriculture. The station is part of the Snotel remote sensing network operated and maintained by NRCS (http://www3.wcc.nrcs.usda.gov/snotel/SNOTEL_brochure.pdf). The NRCS website does not disclose details on the measurement instrument for snow depth.

6.2 Results

I retrieved the data loggers on June 20, 2014. Upon arrival at the study site, I observed that the electrical box containing the data loggers had fallen from the cliff. The four channel logger contained a complete hourly temperature record for the entire period of the installation. However, the two channel logger ceased recording after 0800 on December 16, 2013. This logger contained the temperature record for the rock surface and sensor 3 (Fig. 14). The channel for sensor 3 started recording again at 0900 on January 19, 2014, and continued recording normally for the duration of the installation. The data logger deployed in the tree recorded hourly atmospheric temperature throughout the period of the installation.

Figure 15 shows the complete temperature record from October 15, 2013, until March 31, 2014. Figure 15a in the figure shows the atmospheric temperature, Figure

15b shows the rock surface temperature and sensors 1 and 3 (note the rock surface and sensor 3 records are incomplete due to the failure of the U23 data logger), Figure 15c shows the temperature in the river and sensors 2 and 4), and Figure 15d shows snow depth. There is an overall cooling trend from late October until mid-December with the coldest air temperatures of the winter occurring in the first half of December (Fig. 16). Another period of exceptionally cold temperatures occurred during the first week of February (Fig. 17).

The temperature response of the rock to the cold climate is complex. The temperature record of sensors 2 and 4 declined steadily during the cooling from October to early December (Fig. 15c). There was minimal diurnal fluctuation in temperature in both sensors. Sensor 2 reached a temperature of ~2.0 °C during the December cold period and remained at that temperature until mid-January when it began gradually cooling, reaching a minimum temperature of ~1.6 °C in early April. There was no significant decline in temperature of sensor 4 from the February cold period (Fig. 16c). The temperature at sensor 4 reached 2.0 °C on January 8, 2014, approximately one month later than the deep hole on the ramp (Fig. 15c). There was a muted response to the February cold period during which temperatures as low as ~1.6 °C were recorded by sensor 4 (Fig. 17c).

The response of the rock surface sensor, sensors 1, and 3 was more complex. The temperatures at both sensors 1 and 3 decline during cold period in December, although response from sensor 1 was muted in comparison to the response of sensor 3 (Fig. 16b). Temperatures of sensor 3 were within the frost cracking window during the period December 4-14 (Fig. 16b). This was the only period during which frost cracking temperatures were recorded during the study. During October the daily maximum and minimum temperatures showed little variability with a consistent phase shift of ~5 hr from rock surface temperatures (Fig. 15b). The temperatures from the rock surface sensor were in phase with atmospheric temperatures, but the amplitude of the diurnal fluctuation for the rock surface was consistently less (Fig. 16a and 16b). During the period of December 9-12, the diurnal signal in the rock surface temperature is very muted (Fig. 16b). During the coldest periods of February and March 2014, sensor 3 was the only location recording a significant decline in subsurface rock temperature (Fig. 17b).

The daily river temperature generally fluctuated in a narrow range of ~0.08 < T < ~0.2 °C from early November 2013 to March 2014 (Fig. 15c). Only during one period in the winter of 2013/2014, did the river sensor record sustained temperatures of ~0 °C: February 18 at 1200 PST until February 24 at 0300 PST. During this period river temperature was within 0.051 < T < 0.078 °C, a range which is slightly less than the resolution of the sensor (±0.03 °C). This period also had the highest snow accumulation (Fig. 17d) of the winter. The river began a gradual warming trend in March 2014 (Fig. 15c).

6.3 Interpretations

What explains the short duration that the subsurface rock temperature was within the frost cracking window (Fig. 1)? Rock temperature for sensor 3 (Fig. 14) entered the frost cracking window for several days during the December 2013 cold period (Fig. 16b). This finding is consistent with the solutions of equation (1) for this elevation. However, the amount of time spent in the frost cracking window was substantially less than the prediction of equation (1) at this depth. The winter of 2013/2014 was relatively warm, producing on three brief periods of sustained cold weather (Fig. 15a). Another indication of the warmth of this winter is that the average temperature for the twelve month period beginning July 1, 2013, was 5.51 °C (Fig. 18). The long range *MAT* for this elevation derived from equation (2) is 3.25 °C. If 5.51 °C were the *MAT*, equation (2) would yield an elevation of 2300 masl. This elevation is below the regional threshold to produce rock temperatures within the frost cracking window.

How should the diurnal fluctuation of the river temperature be interpreted? The diurnal fluctuation during most of the winter exceeds the minimum resolution of the sensor (± 0.03 °C). It was only during the period February 18-24 that the diurnal temperature fluctuation was less than the minimum resolution. Given that the mean river temperature during this period was ~0.06 °C and the accuracy of the sensor is ± 0.2 °C, I interpret the constant temperature as an indication that the water in the river at the depth of the sensor was in solid state. During the balance of the winter, the varying daily temperatures suggest that the river was undergoing change of phase. Hence, there was a potential reservoir of liquid water to support frost cracking (water below the depth of the sensor could be warmer). However, the temperature of the river always exceeded the upper bound of the frost cracking window (Fig. 1). Therefore, it also serves as a source of heat, which can affect the temperature of the rock below the surface (Figs. 20, 21).

How should the relatively constant temperature of sensors 2 and 4 be interpreted? The temperature record of sensors 2 and 4 (Fig. 14) both reached ~2.0 °C in early January 2014, and stabilized at around that level through the end of March (Fig. 15). Both sensors were emplaced at a similar depth ~1.0 m. Solutions to equation (1) do not yield stable temperatures at depths < 10 m (Figs. 6, 7a). Even if we assume that snow cover keeps the surface at both locations at ~0.0 °C and that the geothermal gradient is negligible at depths < 20 m (a Hales and Roering (2007) assumption) the rock should continually lose heat to the colder surface. A possible explanation for the constant temperatures at depth ~1.0 m below the surface is a flux of unfrozen ground water. The rock mass itself could be the source of heat needed to maintain the temperatures at sensors 2 and 4.

How should the contrast of the temperature fluctuations of sensors 1 and 3 during December 2013 (Fig. 16b) be interpreted? The temperature record of sensor 1 from the December cold period does not show a clear signal of the cold rock surface temperatures (Fig. 16b). The sensors 1 and 3 were at a similar depth below the surface (Fig. 14), and examination of the cores shows uniform lithology at all locations in the study site (Fig. 14). Hence, differences in thermal diffusivity (Appendix D) do not account for the difference in the two signals. A possible explanation for this difference is snow cover, which has been shown to have an insulating effect (Lundquist and Cayan, 2007). The variability of temperature at sensor 1 decreases significantly (Fig. 16 b) as the snow accumulation increases on December 3 and 4, 2013 (Fig. 16d). The different response of sensors 1 and 3 during the first few days of the cold period can be explained by the ~30 cm of the snow cover (Fig. 16d) as measured at the Ebbetts Pass stations (Fig. 1). If this amount of snow cover were present at the NFM site, it likely would have blanketed the ramp, but it is unlikely that it reached the level of the rock surface sensor which continued to show a strong diurnal signal through December 6, demonstrating the direct influence of the cold atmospheric temperatures. Hence, the cliff face, where sensor three was emplaced ~100 cm above the rock surface sensor (Fig. 14) was exposed to the cold atmospheric temperatures. In addition, the snowfall that began on December 6 doubled the snow cover to a maximum of ~60 cm. The brief flatlining of the rock surface temperature record may indicate snow drifting over the location of that sensor, which was located just above the intersection of the ramp and the cliff (Fig. 14). Thus, these observations show the effect of channel morphology on rock temperatures.

7.0 THE 2D FINITE ELEMENT HEAT FLOW MODEL

The NFM temperature study shows that the climatic parameters of equation (1) are not sufficient to account for the observed temperatures in the rock. Equation (1) only accounts for the long-term impact of the climate on subsurface rock temperature. I developed a 2D model to simulate the heat flows through a cross-section of the channel, in order to more completely account for varying boundary conditions at the surface and the effect of channel morphology. In the modeling, I seek to answer the following questions: How do the river and rock surface temperatures affect the subsurface rock temperature? I hypothesize that surface boundary conditions primarily affect near surface rock temperatures (sensors 1 and 3). What heat flows into the model space are required for the model to produce the relatively warm temperatures of sensors 2 and 4? I hypothesize that heat flow from the rock mass below and to the right of the model space is needed to sustain the recorded temperatures of sensors 2 and 4. What is the effect of insulating snow cover? I hypothesize that snow cover explains some of the observed difference in the record of sensors 1 and 3.

The model solves the 2D heat equation using the finite element method of numerical approximation.

$$\frac{\partial T}{\partial t} = \alpha \nabla^2 T \qquad (3)$$

The parameter α is thermal diffusivity (Appendix D) and ∇^2 is the Laplace operator. One of the principal advantages of the finite element method is that it is readily adaptable to complex geometries, which are prevalent at channel margins.

I used Matlab's PDE toolbox to implement the method. Given a specified geometry for the model space and a set of boundary and initial conditions, the toolbox automatically generates a triangular mesh (Fig. 19) for the finite element calculations. The mesh can be successively refined to arrive at an optimal tradeoff between precision and processing time. A limitation of the PDE toolbox is that it does not accommodate time-dependent boundary conditions. I adjusted the modeling to this limitation by using short time periods during which I set boundary conditions using mean temperature values. Appendix E summarizes the key input screens in the PDE toolbox.

7.1 Methods

My model was designed with the objective of simulating the measured temperatures of the December 2013 cold period, during which the subsurface rock temperature of sensor 3 spent several days in the frost cracking window. During this period, there is also a complete record of the rock surface temperature through December 15. I break the onset of this cold period into two time periods. The model was programed to calculate the temperature distribution in the model space hourly. The first period is the 24 hours, commencing 1900 on December 2. During this period rock surface temperature declined steadily from 0.84 to -3.51 °C (Table III) and averaged -1.02 °C. The second period was the succeeding 76 hours, during which rock surface temperature fluctuated diurnally within a range of ~-2.5 and ~-9.0 °C (Fig. 16b). Mean rock surface temperature during the second time period was -6.54 °C. The boundary conditions used in the modeling are summarized in Table IV. The boundary covered by the river was set to recorded river temperature, which did not fluctuate significantly. The boundary condition for the ramp surface was set at average rock surface temperature during the first period and not changed during the second period due to the assumed effect of snow insulation. Because the recorded temperature at sensor 3 actually increased during the first period, I set the surface boundary condition at T = 0.0 °C. During the second period I set the cliff surface temperature to average rock surface temperature. Through trial and error, I determined that constant temperature boundary conditions at the lower and right hand boundaries of the model space (Figs. 20, 21) were needed to produce the relatively warm temperatures of sensors 2 and 4, i.e. that there was heat flow into the model space across the lower and right boundaries. The initial temperatures at sensors 2 and 4 were 2.45 and 4.25 °C, respectively. I reasoned that the rock must have been warmer at greater depths from the rock surface and set the right boundary condition at T = 6.0 °C and the lower boundary condition at T = 4.0 °C.

The model results at the conclusion of each time step are summarized in Figures 20 and 21. Note that the temperature scales and contour intervals differ in each figure. The PDE toolbox automatically sets the temperature scale to reflect the boundary conditions and calculated temperatures of each iteration. The plot function of the PDE toolbox allows for the selection of the number of contours to display rather than the contour interval.

7.2 Results

The model results for the first time step, the 24 hours ending December 3 at 1800, and (Fig. 20) match the data (Table III) only in part. The modeled values for sensors 1 and 3 approximate the values in Table III. The model isotherms near the river clearly show the reduced heat loss from the rock mass in comparison with the contours below the ramp. This difference is attributable to the warmer boundary condition at the river. The modeled values at sensors 2 and 4 are both somewhat cooler than the actual values at the end of the first time step. A possible explanation for the discrepancy is that the modeled heat flows across the lower and right boundaries of the model were inadequate to maintain the temperatures at the two deep sensors.

Alternatively, the use of fixed boundary conditions for the ramp and cliff surfaces may have the effect of exaggerating the heat loss from the rock mass.

The second period in the modeling was the 76 hour period ending on December 6 at 2200 (Fig. 21). The modeled values for sensors 1 and 3 are good approximations of the values at the end of period, -1.30 °C for sensor 1 and -4.17 °C for sensor 3. I attribute the warmer temperature at sensor 1 to the insulating effect of the snowfall which occurred beginning December 3 (Fig. 16d). This interpretation is consistent with the observation of Matsuoka (2007) that lack of short term fluctuation in near surface rock temperature correlates with snow cover. This effect is captured by the use of a warmer boundary condition on the ramp, where the snow accumulation was likely to be greatest. It is also noteworthy that the average river temperature was ~0.06 °C warmer than it was during the period of the first time step. This may also be attributable to snow accumulation. As with the earlier period, the modeled temperatures at sensors 2 and 4 are cooler than the actuals temperatures of 2.13 °C and 3.83 °C, respectively. The previous comments regarding the potential reasons for this discrepancy are also applicable here.

7.3 Implications

The 2D model highlights the insulating effect of the river and snow cover. The model shows a clear heat signature of the river in the isotherms which show less heat loss to the river than to the colder surfaces of the ramp and cliff (Figs. 20, 21). This contrast between the warmer river temperature and the rock surface exposed to the colder air temperatures shows that the river can have a similar insulating effect to that of snow accumulation. A second insulation effect is illustrated by the contrasting temperature record of sensors 1 and 3 during the period of the modeling. In order for the model to approximate the values in the data, a warmer boundary condition was needed on the ramp surface (Table IV). The different response of sensor 1 in the two periods of the model could be explained by the ~30 cm increase in snow depth on December 3 (Fig. 16d). There was some snow in the area from early November (Fig. 15d). Hence, there may be some minimum snow accumulated needed to fully insulate the rock surface.

The modeling also suggests that there is a heat source within the rock, a possibility not captured by the Hales and Roering (2007) model. The 1D heat model of equation (1) does not account for subsurface heat sources and does not predict stable temperature at depths less than ~10 m (Fig. 6b). The 2D modeling also shows that heat flow from great depth below the surface of the rock mass is needed to produce the warm temperatures in the record of sensors 2 and 4. Alternatively, ground water could be the source of heat, assuming the subsurface fracture network allows for sufficient transport. However, assuming the top of the water table is at the surface of the river, at least sensor 2 would be within the water Table (Fig. 14). Due to the cold temperature of the river a source of heat is still needed to explain the temperatures of sensors 2 and 4. Without the heat flow into the model space, which is set by the lower and right boundary conditions, the model produces much colder temperatures at the depth of sensors 2 and 4. The insulation of increasing snow accumulation would also decrease the rate of heat loss at the rock surface. Hence, the ensuing period of stable temperatures of sensors 2 and 4 (Fig. 15c) could be the result of an equilibrium state between insulation at the surface and a heat reservoir at depth. The slow cooling during the late winter months (Fig. 17c) at these locations to ~1.6 °C may be the result of gradual loss of stored heat by the rock mass.

The ability of the finite element method to accommodate complex geometries and variable boundary conditions at each surface of the model space enables the 2D modeling to be used as a tool to explore how varying climate conditions and channel morphology impact the rock temperature profile. As an illustration, I have developed a generic model of a v-shaped channel (Fig. 22). The current state of the model can be improved with further development. In particular, it should be possible to program time-periodic boundary conditions in the Matlab command space. The use of such boundary conditions would be a significant enhancement, which could bring the results of the model into closer conformity to the internal temperature record of the rock mass and enhance the usefulness of the model in the exploration of the influence of the river in varying settings.

8.0 DISCUSSION

I began this study with the question of whether frost cracking occurs in the bedrock banks of alpine rivers. I have shown that a bedrock bank on the NFM reached subsurface temperatures within the frost cracking window at an elevation ~150 m above the minimum predicted elevation for the central Sierra Nevada range, during an unusually warm winter. What can be said about the role of the river? At the NFM study site, the modeling show that it supplies heat, which suppresses frost cracking. But the temperature record of the river during the warm winter of 2013/2014 also shows that it was a source of liquid water. If the water table contains liquid water, it could support frost cracking in the bedrock hillslope, which is just a few meters distant from the low flow channel.

Notwithstanding the progress made towards the understanding of segregation ice by my study, there remain several important unanswered questions. What can be expected to occur at higher elevations where the climate can be expected to promote greater frost cracking intensity? Is there liquid water available? I have speculated that water may be advecting heat at the NFM site. Could the same advection occur at higher elevations, permitting the transport of water to nearby hillslopes where the rock temperatures are in the frost cracking window? Extension of the 2D finite element modeling is one way to explore answers to these questions.

The Tuolumne portion of my study shows that lithology may be an important factor in determining susceptibility of rock to frost cracking. Only the Kcp member of the TIS exhibited a joint pattern that could be indicative of frost cracking. Although it is not clear why the other plutonic rock in the region does not display greater joint density at the river margin, I note that each member of the TIS has a unique geochemistry and magmatic alignment of crystalline structure (Zak et al., 2007). These differences must translate into different zones of weakness along grain boundaries and thus, different susceptibility to fracturing and jointing. Do pre-existing fractures due to tectonic or topographic stress contribute to frost cracking susceptibility? It would seem to be the case, since pre-existing fractures provide more pathways for water to enter the rock mass. Topographic stress would seem to favor fracturing of bedrock banks because stress is concentrated at the base of hillslopes (Miller and Dunne, 1996).

How can we distinguish fractures and joints cause by frost cracking from those caused by other forms of weathering? I think it is difficult, but at least we can say that frost cracking should be evidenced by opening mode fractures. Sometimes evidence of fracture mode can be discerned in the field. In addition, from my early thinking on the subject of my study, I have believed that greater fracture or joint density in proximity to water in alpine landscapes is indicative of frost cracking. I believe that the Kcp jointing on the Tuolumne is an example. Matsuoka (2007) also found that frost shattered rock was more prevalent near lakes and streams in the Swiss Alps.

The modeling of my study helps to highlight the importance of snow accumulation. I have shown that snow cover insulates both rock and river from cold atmospheric temperatures, keeping subsurface rock temperatures above what they would be absent snow cover. By warming the river, snow cover can facilitate the production of liquid water in the channel. How does channel morphology affect snow accumulation? Aspect, bank slope, channel width, and the presence of liquid water must all be factors.

The idea of a penalty for the distance between the source of water and the frozen zone in frost cracking models is a logical extension of existing theory. The study of Anderson et al. (2012) introduced the concept. The authors' model implemented the penalty through the introduction of a length-based exponential decay term into a model similar to equation (1). The weakness in that approach is that the authors did not establish an empirical basis for the decay term. As an alternative to a distance based penalty, the type of 2D modeling in this study could be adapted to reflect differences in the fracture densities of bedrock river beds and banks. The difference could be modeled by the use of subsurface boundary conditions which reflect the higher advective heat flow capacity of water in a dense fracture network in contrast with less porous material.

9.0 SUMMARY AND CONCLUSION

There are many studies in the literature that document the role of frost cracking in breaking bedrock in alpine landscapes (Hales and Roering, 2009; Matsuoka, 2007; Sanders et al., 2012). However, none of the previous studies are focused explicitly on the role that frost cracking plays in the evolution of bedrock river banks. This study is an effort to fill this gap and to contribute to the unsolved problem of how bedrock banks erode (Whipple, 2004). The first question addressed in the study is where in the landscape should I look for evidence of frost cracking? I used the work of Hales and Roering (2007) to predict the zone of frost cracking intensity in the central Sierra Nevada to answer this question (Fig. 8). Using multi-year climate records, I established that the minimum elevation threshold for frost cracking is ~2325 masl in the region of the study. In the next phase of the study I conducted reconnaissance in several watersheds in the central Sierra seeking field evidence for frost cracking on bedrock banks at elevations above 2325 masl. I find a tantalizing, if inconclusive, result by comparing joint densities at the river margin and adjacent hillslopes (Table II) in the Kcp unit of TIS in Yosemite National Park. The statistical significance of the denser jointing at the river margin (Appendix C) indicates that a more intensive mechanical weathering process occurs at the river margin. This result motivated for the temperature study at the NFM study site. In this portion of the study, I established that the subsurface rock temperature does reach the frost cracking window, as predicted by equation (1) for this elevation. The boundary conditions of the finite element 2D heat flow model are informed by the rock surface and river temperatures from the NFM temperature record. Experimentation with other boundary conditions leads to a conjecture regarding heat flow into the model space. The model is able to approximate the temperatures of the sensors with the benefit of assumptions regarding the boundary conditions.

The data from the NFM site shows that equation (1) is an incomplete tool for the prediction of frost cracking. Equation (1) does not account for surface boundary conditions that can vary due to snow cover, aspect of the bank, or the temperature of river water. Finite element 2D modeling allows varying the boundary conditions to reflect the influence of these factors and channel morphology (Fig. 22).

This study does not definitively answer the central questions of whether segregation ice is a mechanism that erodes river banks. Although it shows that the rock at the NFM site enters the frost cracking window for a few days in December 2013 (Fig. 16), it does not confirm that there is liquid water near the location (Fig. 14) where those temperatures are recorded. However, the study is ongoing. In September 2014, we set up the instrumentation at the NFM site to gather temperature data for winter

2014/2015. The sensor configuration is similar to that of the previous winter, except that we have substituted Decagon sensors at locations 3 and 4 (Fig. 14). In addition, to recording temperature, these sensors can also detect the presence of water.

There are two additional areas of ongoing work. In October 2013, we conducted a ground based LiDAR scan of the bedrock bank at the NFM site with the assistance of the US Geological Survey. The scan produced a mm-scale representation of the channel margin. Later this year, we hope that this resource will become available for a second scan. The second scan would enable mapping of changes in the channel morphology and an estimation of erosion rate. Secondly, I am continuing refinement of the finite element 2D model. In addition to refining some of the mechanics of the model, such as introducing time-periodic boundary conditions, I plan to extend the use of the model to varying scenarios of elevation and channel morphology. These efforts will hopefully extend the insights gained in this study.

REFERENCES

Albertz, Markus, SR Paterson and D Okaya (2005); Fast strain rates during pluton emplacement: Magmatically folded leucocratic dikes in aureoles of the Mount Stuart Batholith, Washington, and the Tuolumne Intrusive Suite, California; *GSA Bulletin*; 117, no. 3-4; 450-465.

Anderson, Robert S, SP Anderson and GE Tucker (2012); Rock damage and regolith transport by frost: an example of climate modulation of the geomorphology of the critical zone; *Earth Surface Processes and Landforms*; DOI: 10.1002/esp.3330.

Armin, Richard A, DA John, WJ Moore and JC Dohrenwend (1984); Geologic map of the Markleevile 15 minute quadrangle, Alpine County, California; US Geological Survey.

Bateman, Paul C. and BW Chappell (1979);Crystallization, fractionation, and solidification of the Tuolumne Intrusive Series, Yosemite National Park, California; *GSA Bulletin*; 90, no. 5; 465-482.

Bateman, Paul C, RW Kistler, DL Peck, and A Busacca (1983); Geologic map of the Tuolumne Meadows quadrangle, Yosemite National Park, California; US Geological Survey

Degraff, James M. and A Aydin (1987); Surface morphology of columnar joints and its significance to mechanics and direction of joint growth; *GSA Bulletin*; 99, no. 5; 605-617.

Duvall, Alison, E Kirby and D. Burbank (2004); Tectonic and Lithologic controls on bedrock channel profiles in coastal California; *Journal of Geophysical Research*; 109, F03002.

Drury, MJ (1987); Thermal diffusivity of some crystalline rocks; *Geothermics*; 16, no. 2, 105-115.

Duvall, Alison, E. Kirby, and D. Burbank, (2004); Tectonic and Lithologic controls on bedrock channel profiles and process in coastal California; Journal of Geophysical Research; 109, F03002.

Finnegan, Noah J, LS Sklar and TK Fuller (2007); Interplay of sediment supply, river incision, and channel morphology revealed by the transient evolution of an experimental bedrock channel; *Journal of Geophysical Research*; 112, F03S11.

Gilpin, RR (1980); A model for the prediction of ice lensing and frost heave in soils; *Water Resources Research*; 16, no. 5; 918-930.

Glazner, Allen F and GM Stock (2010); Geology under foot in Yosemite National Park; Mountain Press Publishing Co., Missoula, Montana.

Hales, TC and JJ Roering (2007); Climate controls on frost cracking and implications for the evolution of bedrock landscapes; *Journal of Geophysical Research*; 112, F02033.

Hales, TC and JJ Roering (2009); A frost "buzzsaw" mechanism for erosion of eastern Southern Alps, New Zealand; *Geomorphology*; 107, 241-253.

Hallet, B. JS Walder and CW Stubbs (1991); Weathering by segregation ice growth in microcracks at sustained sub-zero temperatures: Verification from an experimental study using acoustic emissions; *Permafrost and Periglacial Processes*, 2, 283-300.

Lundquist, Jessica D and DR Cayan (2007); Surface temperature patterns in complex terrain: Daily variations and long-term change in the central Sierra Nevada, California; *Journal of Geophysical Research*; 112, D11124.

Matsuoka, Norikazu (2007); Frost weathering and rockwall erosion in the southeastern Swiss Alps: Long-term (1994-2006) observations; *Geomorphology*; 99, 353-368.

Miller, Daniel J and T Dunne (1996); Topographic perturbations of regional stresses and consequent bedrock fracturing; *Journal of Geophysical Research*; 101, no. B11, 25523-25536.

Montgomery, David R and KB Gran (2001); Downstream variations in the width of bedrock channels; *Water Resources Research*; 37, no. 6, 1841-1846.

Murton, Julian B, R Peterson and JC Ozout (2006); Bedrock fracture by ice segregation in cold regions; *Science*; 314, no. 5802, 1127-1129.

Sanders, Johnny W., KM Cuffey, JR Moore, KR MacGregor and JL Kavanaugh (2012); Periglacial weathering and headwall erosion in cirque glacier bergschrunds; *Geology*; 40, no. 9, 779-782.

Scherier, Dirk (2014); Climatic limits to headwall retreat in the Khumbu Himalaya, eastern Nepal; *Geology*; 42, no. 11, 1019-1022.

Vosteen, Hans-Dieter and R Schellschmidt (2003); Influence of temperature on thermal conductivity, thermal capacity and thermal diffusivity for different types of rock; *Physics and Chemistry of the Earth*; 28, 499-509.

Walder, J and B Hallet (1985) A theoretical model of the fracturing of rock during freezing*:* *GSA Bulletin*; 96, 336-346.

Whipple, Kelin X (2004); Bedrock rivers and the geomorphology of active Orogens; *Annual Review Earth Planet. Science*; 32, 151-185.

Whipple, Kelin X, GS Hancock and RS Anderson (2012); River incision into bedrock: Mechanisms and relative efficacy of plucking, abrasion, and cavitation; *GSA Bulletin*; 112, no. 3, 490-503.

Wobus, Cameron W, GE Tucker and RS Anderson (2006); Self-formed bedrock channels; *Geophysical Research Letters*; 33, L18408.

Zak, Jiri, SR Paterson and V Memeti (2007); Four magmatic fabrics in the Tuolumne Batholith, central Sierra Nevada, California (USA): Implications for interpreting fabric patterns in plutons and evolution of magma chambers in the upper crust*;* *GSA Bulletin*; 119, no. 1-2, 184-201.

Table I

Study Area Station Data from CDEC

BASIN[1]	STATION ID[1]	Elevation (m)[1]	*MAT* (°C)[2]
Mokelumne	HHM	2652	3.83
Mokelumne	BLK	2438	4.25
Mokelumne	MDL	2408	5.70
Mokelumne	CVS	1024	12.44
Mokelumne	MTZ	905	15.22
Stanislaus	DDM	2819	2.47
Stanislaus	GNL	2560	5.22
Stanislaus	REL	2469	5.17
Stanislaus	SLM	2362	3.67
Stanislaus	BLD	2195	7.02
Stanislaus	BLS	1982	8.43
Stanislaus	NMS	427	16.32
Tuolumne	TES	3031	1.33
Tuolumne	DAN	2987	1.17
Tuolumne	TMM	2804	2.43
Tuolumne	SLI	2804	1.52
Tuolumne	TUM	2621	2.54
Tuolumne	HRS	2560	1.80
Tuolumne	KIB	2042	8.07
Tuolumne	MTE	1503	12.31
Tuolumne	TLH	1173	14.64
Tuolumne	BKM	975	12.35
Merced	TNY	2482	2.70
Merced	GIN	2149	8.66
Merced	MPG	1951	9.74
Merced	DGH	1859	7.28
Merced	YOW	1511	9.21
Merced	YYV	1280	11.82
Merced	JSD	1189	12.66
Merced	DUC	1114	11.57
Merced	MRP	686	14.92

1. From CDEC station metadata. 2. From equation (2)

Table II

Kcp Joint Spacing

Tuolumne River Bank

Location	Elevation (masl)	Joint spacing (cm)
37° 53.44′ 119° 23.59′	2587	4, 8, 10, 11, 7, 11, 9, 9, 9, 7, 13
37° 53.95′ 119° 54.38′	2574	7, 7, 3, 2, 4, 2, 3, 12, 9
37° 53.33′ 119° 23.39′	2605	12, 9

Hillslopes

Location	Elevation (masl)	Distance from river (m)	Joint spacing (cm)
37° 53.29′ 119° 23.40′	2582	7.6	16, 35, 24, 61, 24, 43, 48, 12, 36, 31
37° 53.92′ 119° 24.52′	2569	4.0	33, 48, 33
37° 53.44′ 119° 23.57′	2589	2.5	16, 12, 30
37° 53.44′ 119° 23.52′	2593	8.5	7, 4, 56, 51
37° 53.39′ 119° 23.45′	2597	8.5	11, 34, 6, 16

Table III

Temperature Record for 24 hr. Period Ending 3 Dec at 1800 (°C)

Day/time	Sensor 1	Sensor 2	Sensor 3	Sensor 4	Surface	River	Atmos.
2 Dec/1900	-1.185	2.45	0.024	4.246	0.825	0.135	1.344
2000	-1.128	2.45	0.051	4.246	0.273	0.135	0.605
2100	-1.071	2.45	0.135	4.246	-0.06	0.135	0.19
2200	-1.043	2.45	0.19	4.22	0.329	0.135	0.632
2300	-1.015	2.423	0.246	4.22	0.439	0.135	0.907
3 Dec/0000	-1.015	2.423	0.301	4.22	0.467	0.135	0.66
0100	-0.986	2.423	0.384	4.22	0.107	0.135	-0.283
0200	-0.986	2.396	0.412	4.22	0.301	0.135	-0.311
0300	-0.958	2.396	0.439	4.194	-0.339	0.135	-1.27
0400	-0.93	2.396	0.439	4.22	-0.62	0.135	-1.785
0500	-0.902	2.396	0.467	4.194	-0.451	0.135	-1.498
0600	-0.873	2.396	0.495	4.194	-0.311	0.135	-1.27
0700	-0.873	2.396	0.495	4.194	-0.563	0.135	-1.527
0800	-0.845	2.396	0.495	4.194	-1.015	0.135	-1.958
0900	-0.817	2.37	0.495	4.194	-1.071	0.135	-2.189
1000	-0.817	2.343	0.495	4.194	-1.842	0.135	-3.094
1100	-0.789	2.343	0.495	4.194	-2.334	0.135	-4.287
1200	-0.76	2.343	0.495	4.194	-2.247	0.135	-5.357
1300	-0.732	2.343	0.495	4.194	-2.218	0.163	-5.791
1400	-0.732	2.343	0.495	4.194	-2.334	0.135	-5.636
1500	-0.704	2.343	0.495	4.194	-2.189	0.135	-6.01
1600	-0.704	2.343	0.467	4.168	-2.625	0.135	-6.738
1700	-0.676	2.343	0.467	4.168	-3.538	0.135	-7.219
1800	-0.648	2.316	0.439	4.194	-3.508	0.135	-10.511
							-10.757

Table IV

Boundary Conditions for 2D Modeling (Figs. 20, 21)

Boundary	24 hrs. starting 1900, 12/2 (°C)	76 hrs. starting 2000, 12/3 (°C)
Rock under river	T = 0.14	T = 0.20
Ramp surface	T = -1.02[1]	T = -1.02[2]
Cliff surface	T = 0.0	T = -6.54[1]
Right boundary	T = 6.0[3]	T = 6.0[3]
Lower boundary	T = 4.0[3]	T = 4.0[3]
Top boundary	T' = 0.0[4]	T' = 0.0[4]
Left boundary	T' = 0.0[4]	T' = 0.0[4]

Notes: 1. Average rock surface temperature for period

2. Assuming no change in ramp surface temperature due to insulation of 30 cm of additional snow cover

3. Heat flow required to produce recorded temperatures of sensors 2 and 4

4. Assumes no heat flow across this boundary

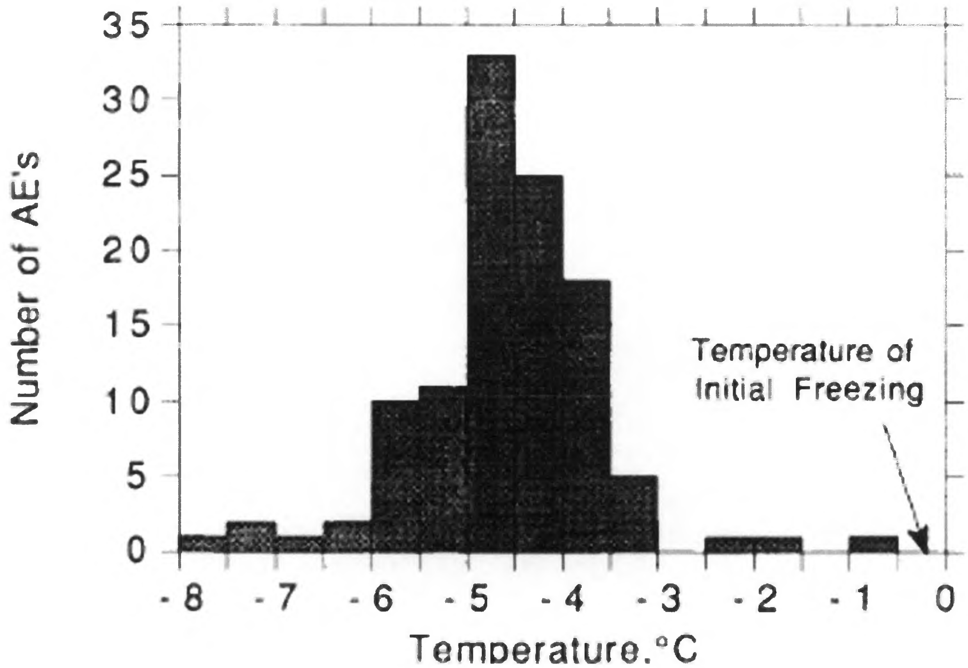

Figure 1. Distribution of acoustic emission (AE's) by temperature (Figure 5 in Hallet et al., 1991). The authors note that the range of most intense AE's (-6 < T < -3 °C) is in accord with the theoretical predictions of Walder and Hallet (1985). This figure is the basis for the prevailing definition of "frost cracking window" -8 < T < -3 °C in the geomorphology literature, e.g. Hales and Roering (2007), Anderson (2012), Sanders et al. (2012), Scherier (2014).

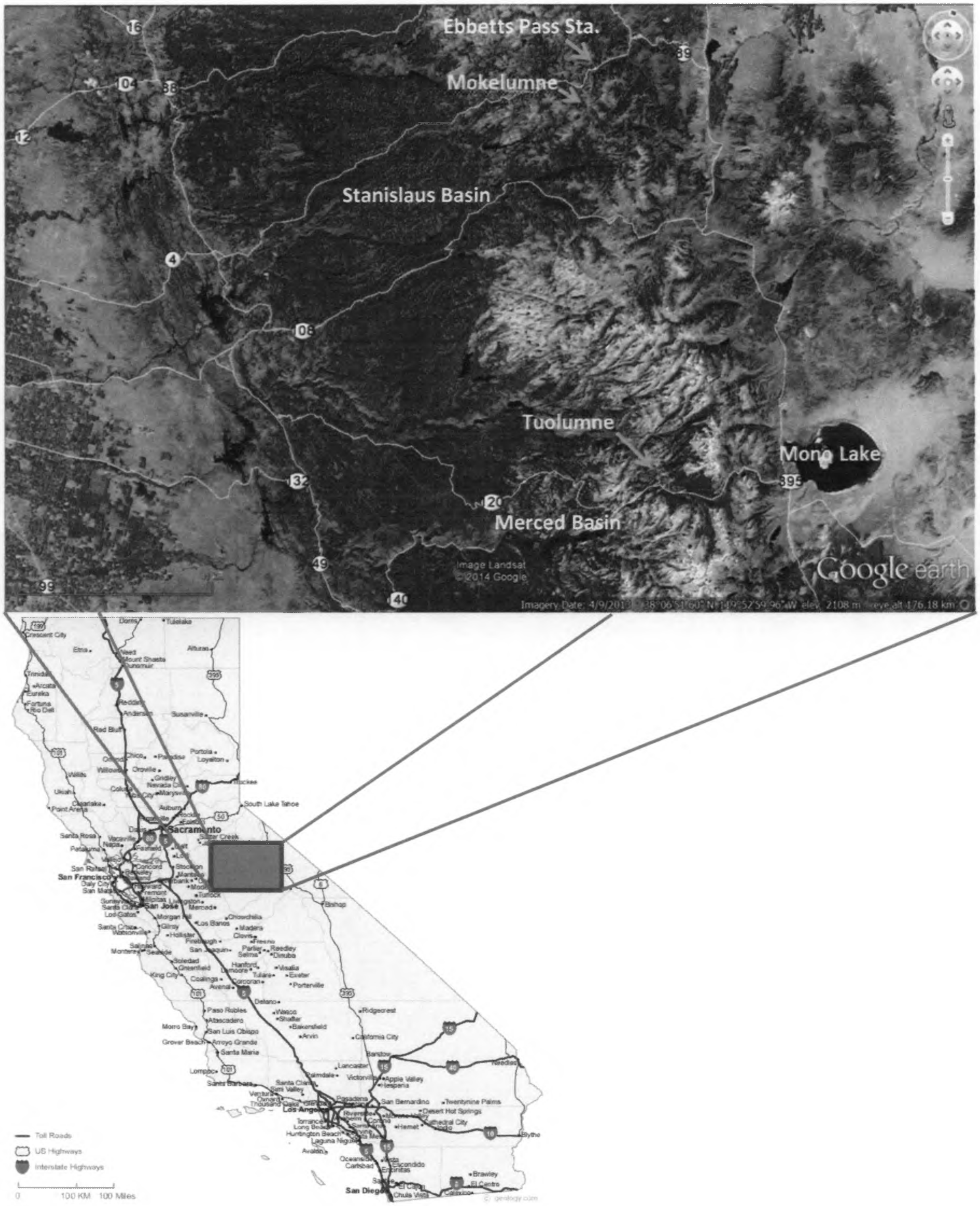

Figure 2. Central Sierra Nevada, California. North Fork Mokelumne and Tuolumne River field sites for the study are marked by the arrows. Location of Ebbetts Pass weather station and other basins used in Section 4 also indicated.

Bivariate Fit of MAT (deg. C) By Elevation (m)

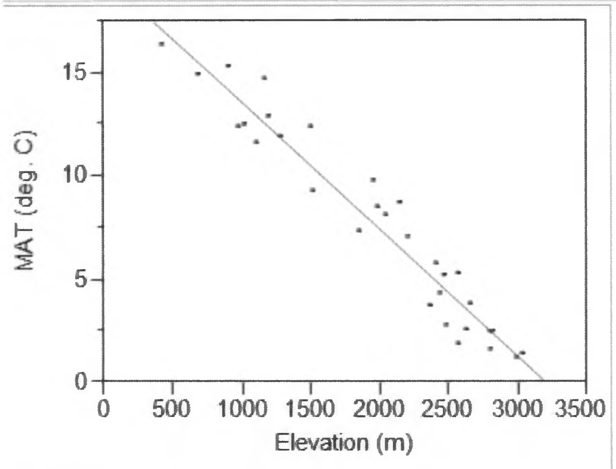

Linear Fit

Linear Fit

MAT (deg. C) = 19.738879 - 0.0061554*Elevation (m)

Summary of Fit

RSquare	0.936638
RSquare Adj	0.934454
Root Mean Square Error	1.224486
Mean of Response	7.634194
Observations (or Sum Wgts)	31

Lack Of Fit

Analysis of Variance

Source	DF	Sum of Squares	Mean Square	F Ratio
Model	1	642.76512	642.765	428.6910
Error	29	43.48164	1.499	Prob > F
C. Total	30	686.24675		<.0001*

Parameter Estimates

Term	Estimate	Std Error	t Ratio	Prob>|t|
Intercept	19.738879	0.624627	31.60	<.0001*
Elevation (m)	-0.006155	0.000297	-20.70	<.0001*

Figure 3. Linear fit of *MAT* versus elevation for all stations included in the study (*Ta*ble II). *MAT* shows strong correlation with elevation. $R^2 = 0.937$. Equation (2) is based on this regression analysis.

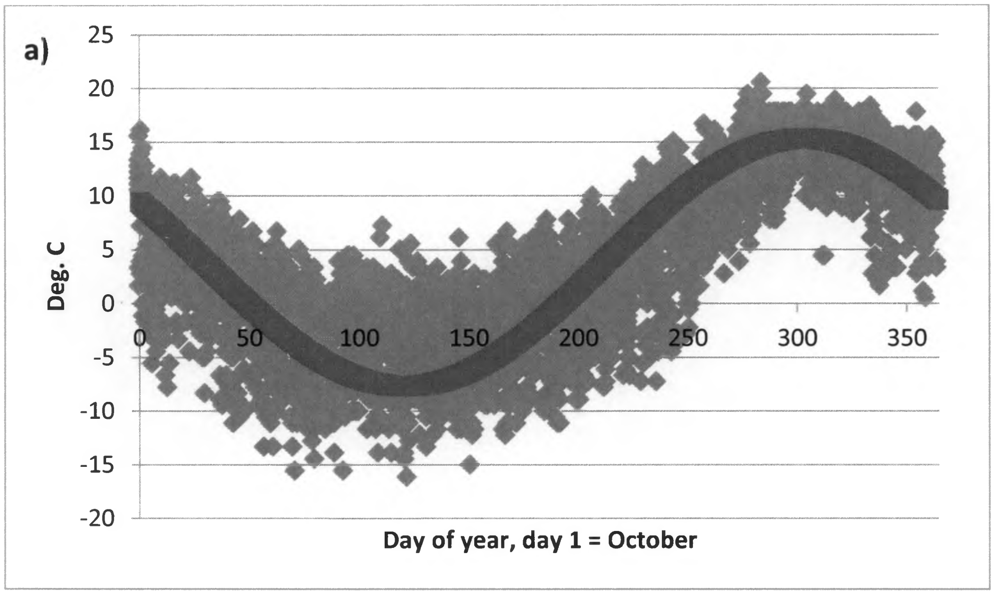

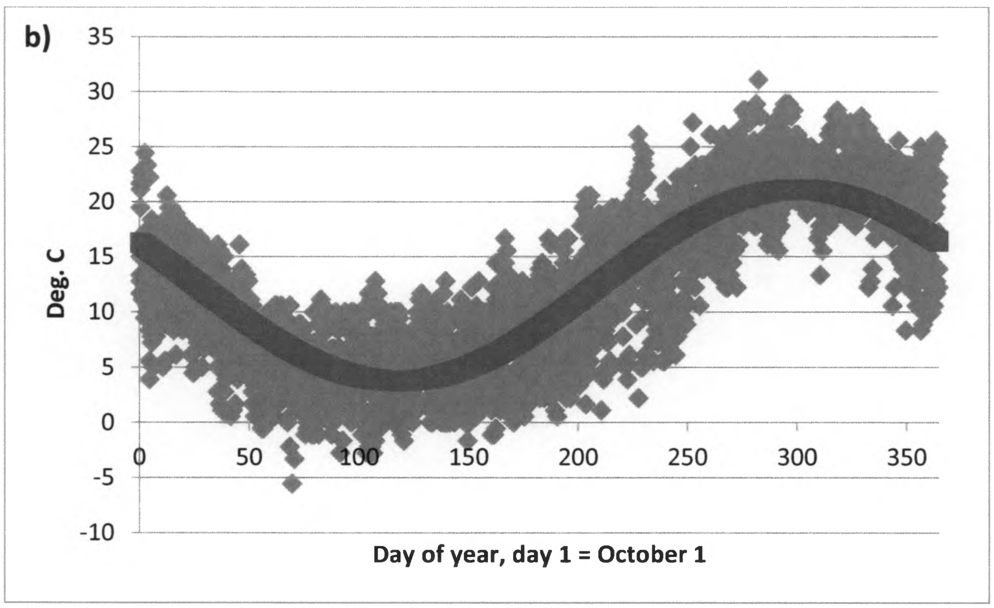

Figure 4. Daily temperature records for two Mokelumne basin stations. **a)** Daily mean temperature plot for a 12 year record beginning 12/1/1999 from the Highland Meadows station (approximately 0.5 km from the Mokelumne study site (Fig. 1)) at elevation 2652 masl. The years beginning 10/1/2004 and 10/1/2005 are excluded due to numerous outliers in the temperature record from the station. The amplitude of the curve, *Ta*= 8.4 °C, minimizes the RMS (4.47 °C) of the difference between the value predicted by the curve and the recorded temperature record for the days with recorded temperatures < 0 °C (days 1 to 250). **b.** Same methodology applied to an 8 year temperature record beginning 10/1/2005 for the Calaveras Ranger Station at elevation 1024 masl. RMS =3.51 °C, *Ta*=8.7 °C.

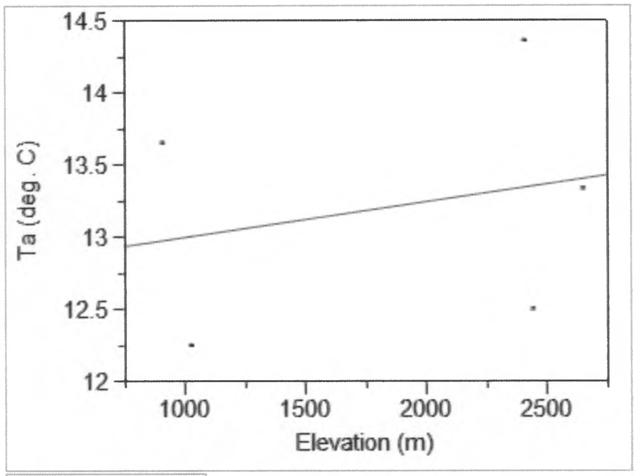

Linear Fit

Linear Fit

Ta (deg. C) = 12.757499 + 0.0002453*Elevation (m)

Summary of Fit

RSquare	0.058368
RSquare Adj	-0.25551
Root Mean Square Error	0.963593
Mean of Response	13.22
Observations (or Sum Wgts)	5

Analysis of Variance

Source	DF	Sum of Squares	Mean Square	F Ratio
Model	1	0.1726640	0.172664	0.1860
Error	3	2.7855360	0.928512	Prob > F
C. Total	4	2.9582000		0.6954

Parameter Estimates

Term	Estimate	Std Error	t Ratio	Prob>|t|
Intercept	12.757499	1.155856	11.04	0.0016*
Elevation (m)	0.0002453	0.000569	0.43	0.6954

Figure 5. Plot of *Ta* values by elevation for selected stations in the central Sierra Nevada. In this case the value of *Ta* is the difference between the 97.5 and 2.5 quantiles of the temperature distributions for each sample station. Linear fit shows no significant correlation with elevation, $R^2 = 0.058$. Hence, *Ta* is constant over the range of elevations in the analysis.

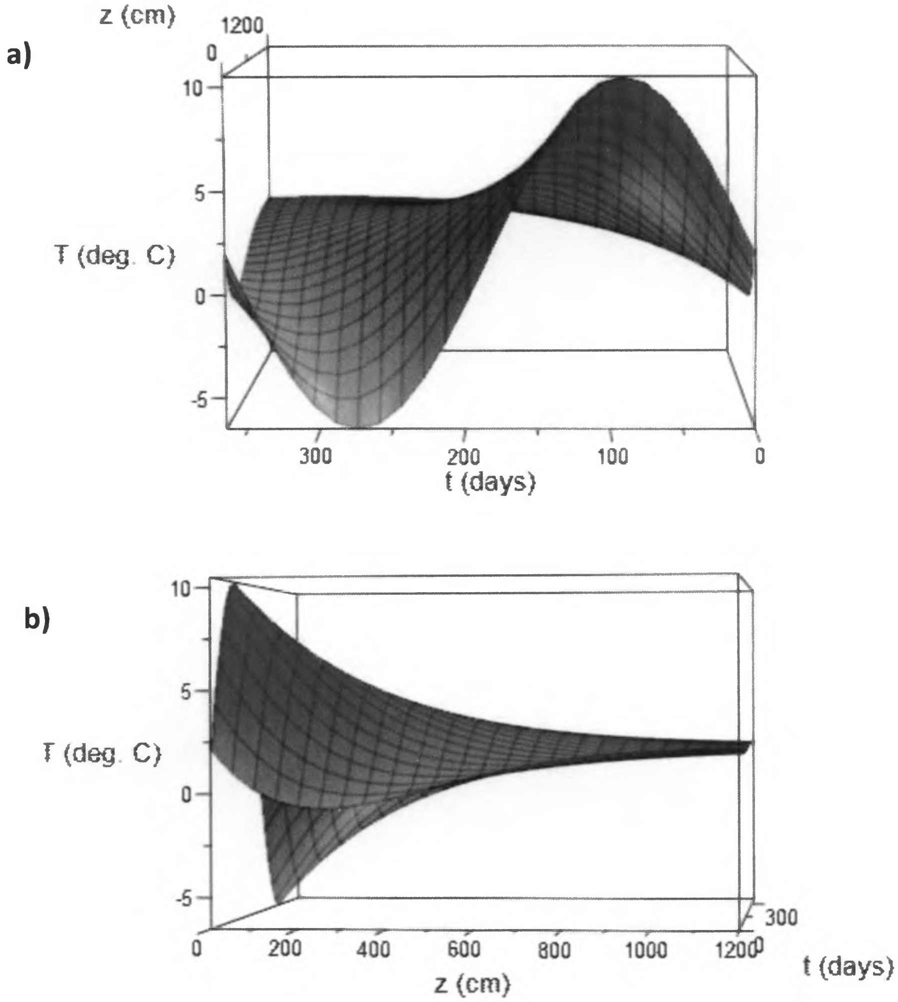

Figure 6. Solutions plot with two perspectives on equation (1) with *MAT* = 2.0 °and *Ta* = 8.5 °C. Day 1 is the first day of spring. Plot **a)** shows the sinusoidal shape of the surface. Plot **b)** is a 90° rotation of plot **a)**, providing a better perspective on the convergence onto a plane at *T* = 2.0 °C.

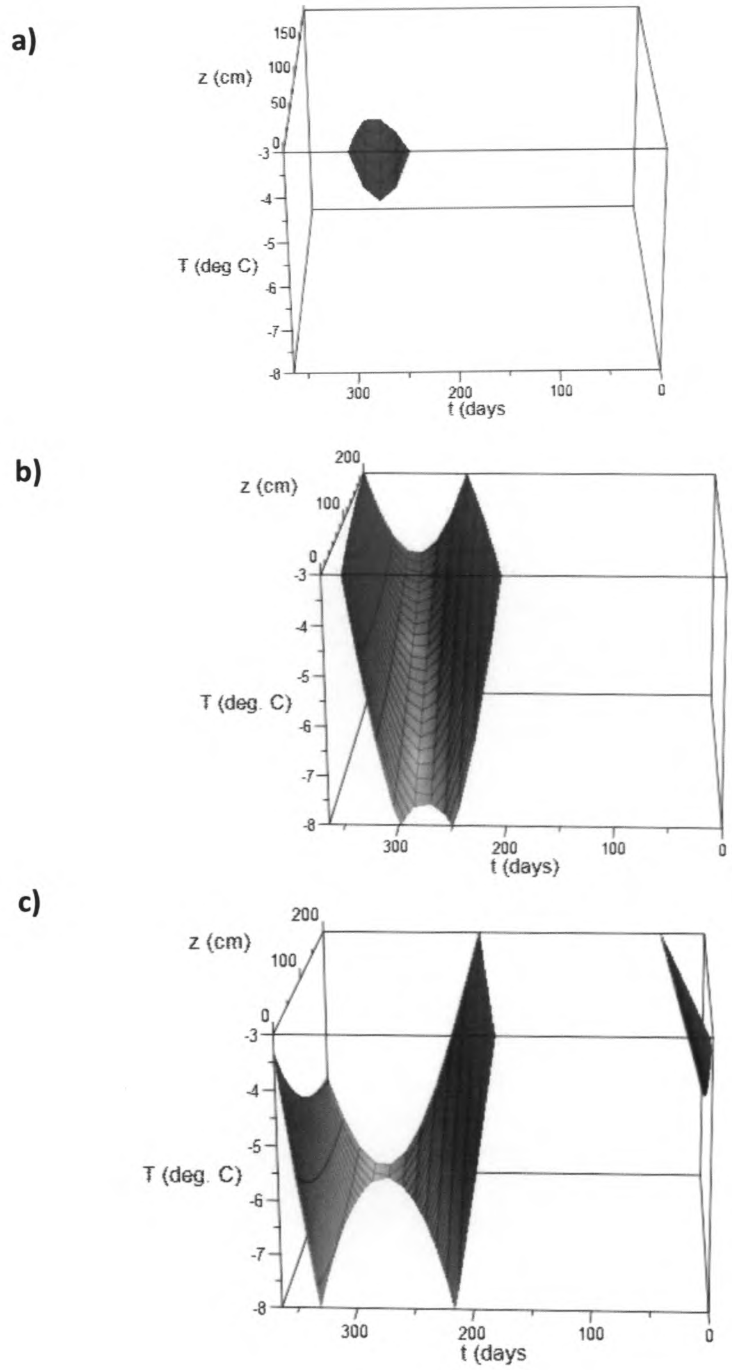

Figure 7. Plots of equation (1) for -8 ≤ T ≤ -3 °C at elevations **a)** 2490 masl, **b)** 3250 masl, and **c)** 3750 masl.

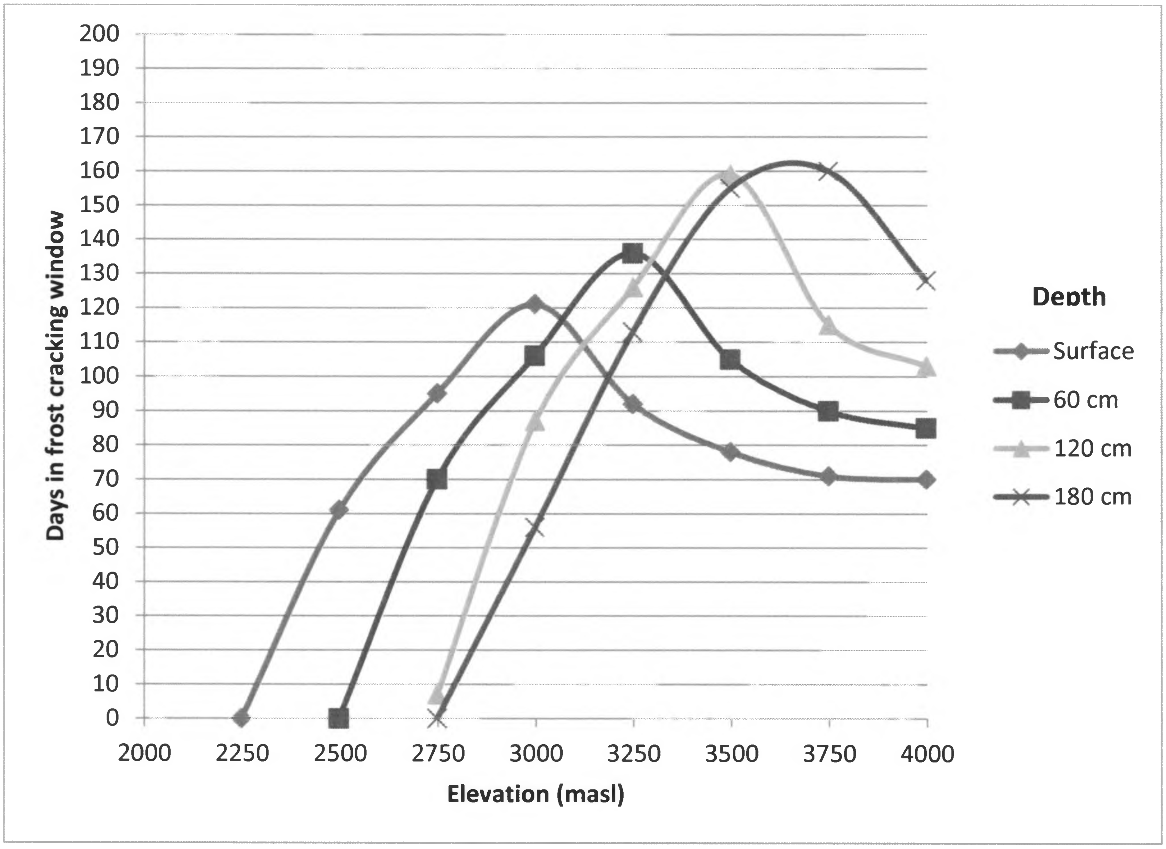

Figure 8. Time spent in frost cracking window as a function of elevation at the surface and indicated depths. Note how depth of maximum duration increases with elevation

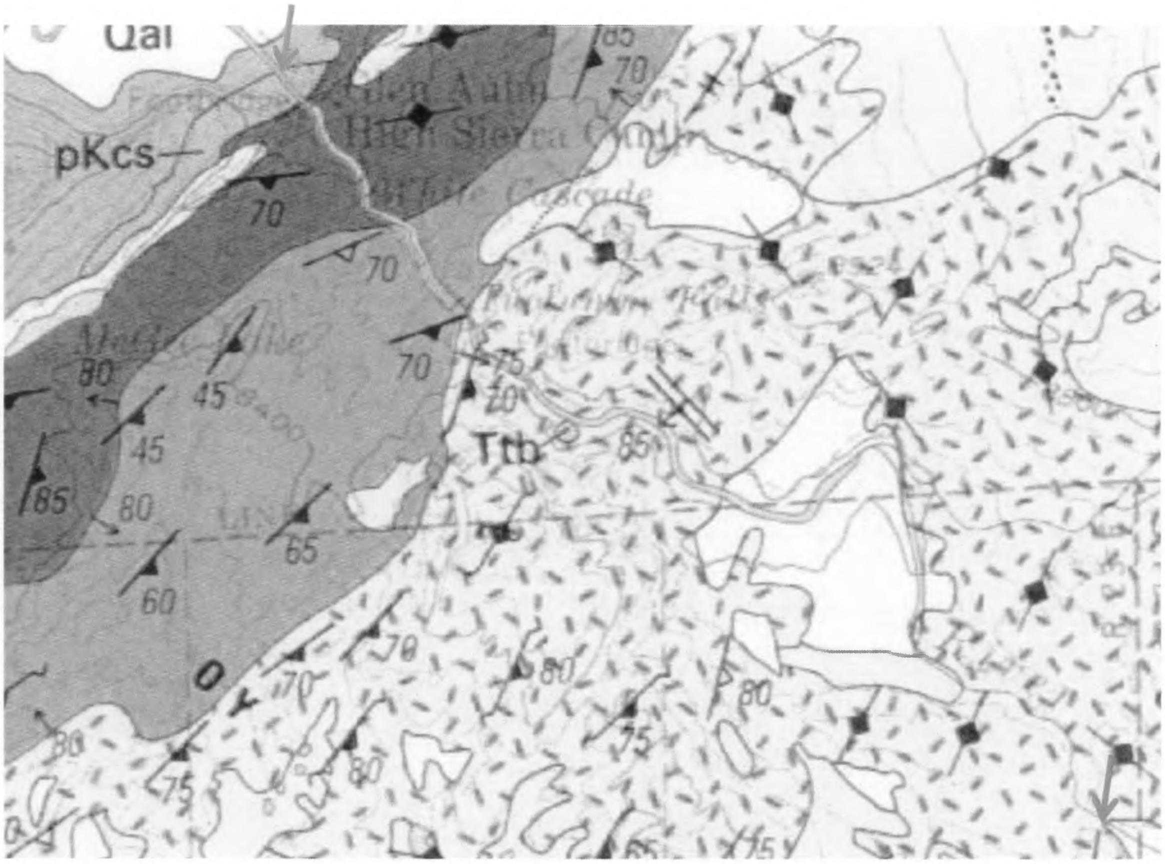

Figure 9. Geologic map of the Tuolumne traverse (end points marked by green arrows). From Bateman et al. (1983). Bedrock map units:

Tuolumne intrusive suite (Cretaceous):

Cathedral Peak granodiorite

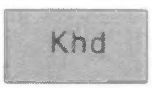

Halfdome granodiorite, equiangular facies

Tonalite of Glen Aulin

Metasedimentary (pre-Cretaceous):

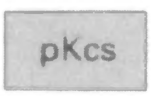

Calc-silicate hornfels, quartzite, and schists

Volcanic plug (Miocene):

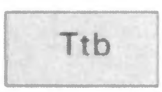

Trachyandesite

a) 

b) 

Figure 10. Surface parallel jointing in Kcp **a)** at the Tuolumne River margin and **b)** on a nearby hillslope.

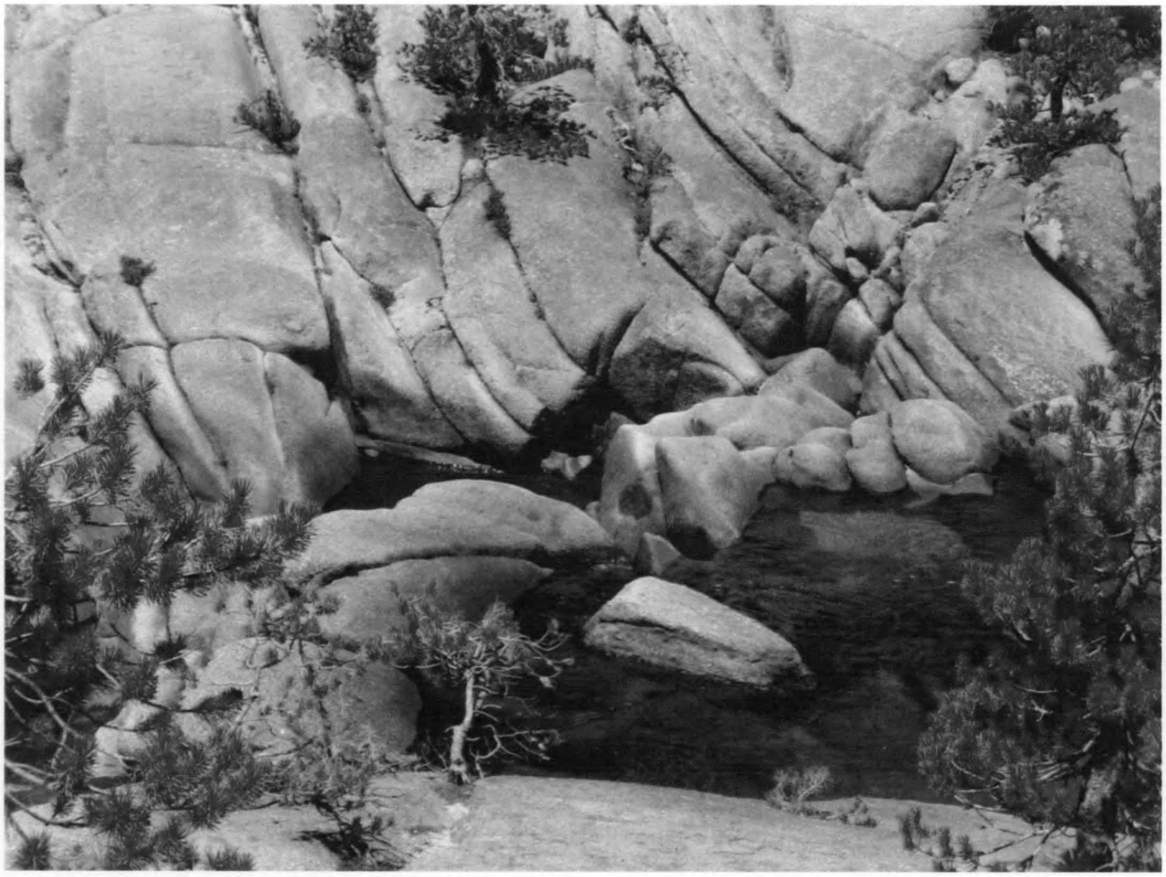

Figure 11. Steeply dipping joints in Khd. Note continuity of the jointing from the river margin to the hillslope.

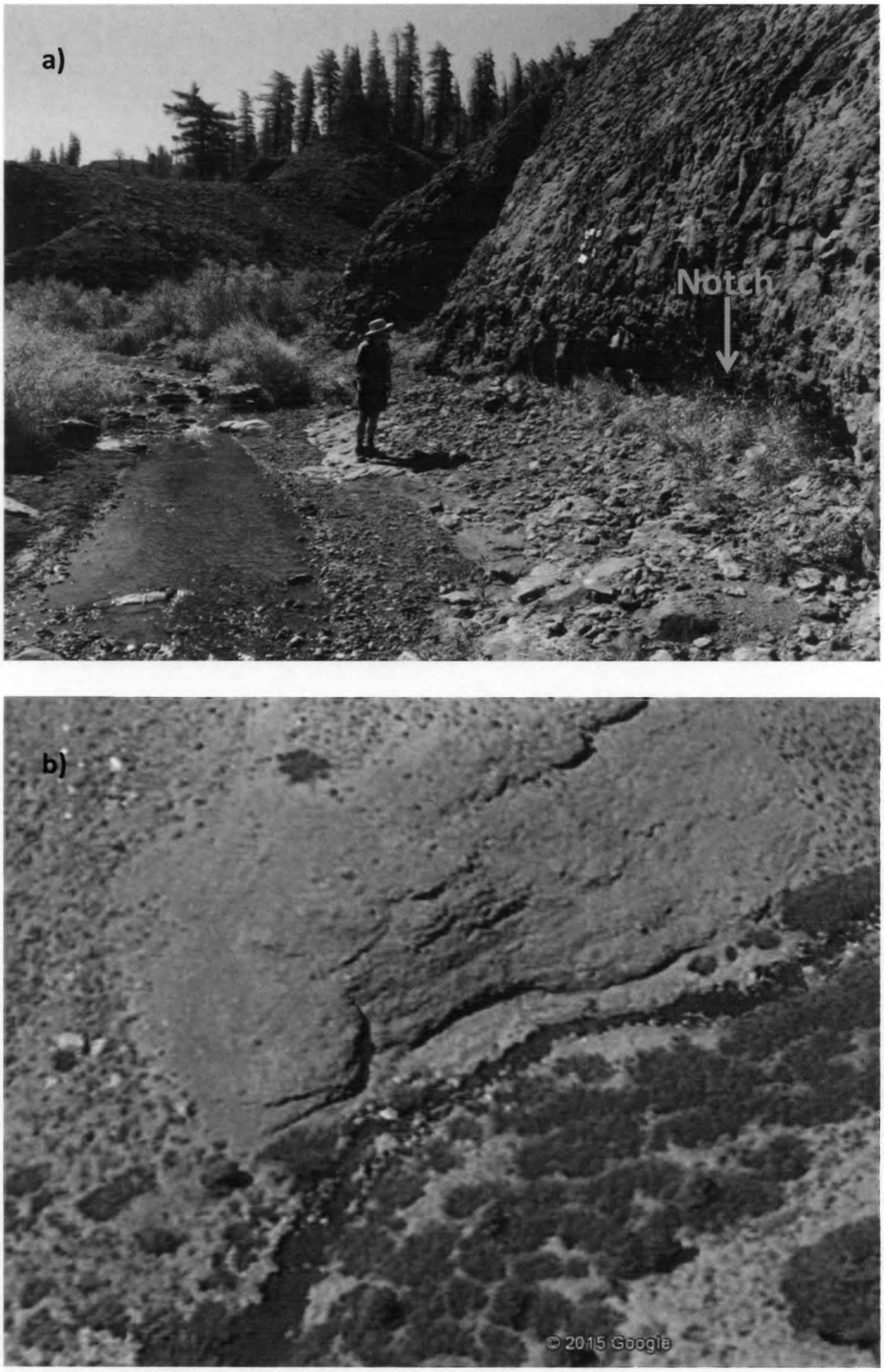

Figure 12. Cliff and ramp morphology at NFM study site. **a)** Ground level view of notch where cliff and ramp meet. **b)** Overhead view from Google Earth. This viewpoint shows curvature of the river. It appears likely that, during spring floods, the river discharge could reach the base of the cliff, causing erosion by clast abrasion.

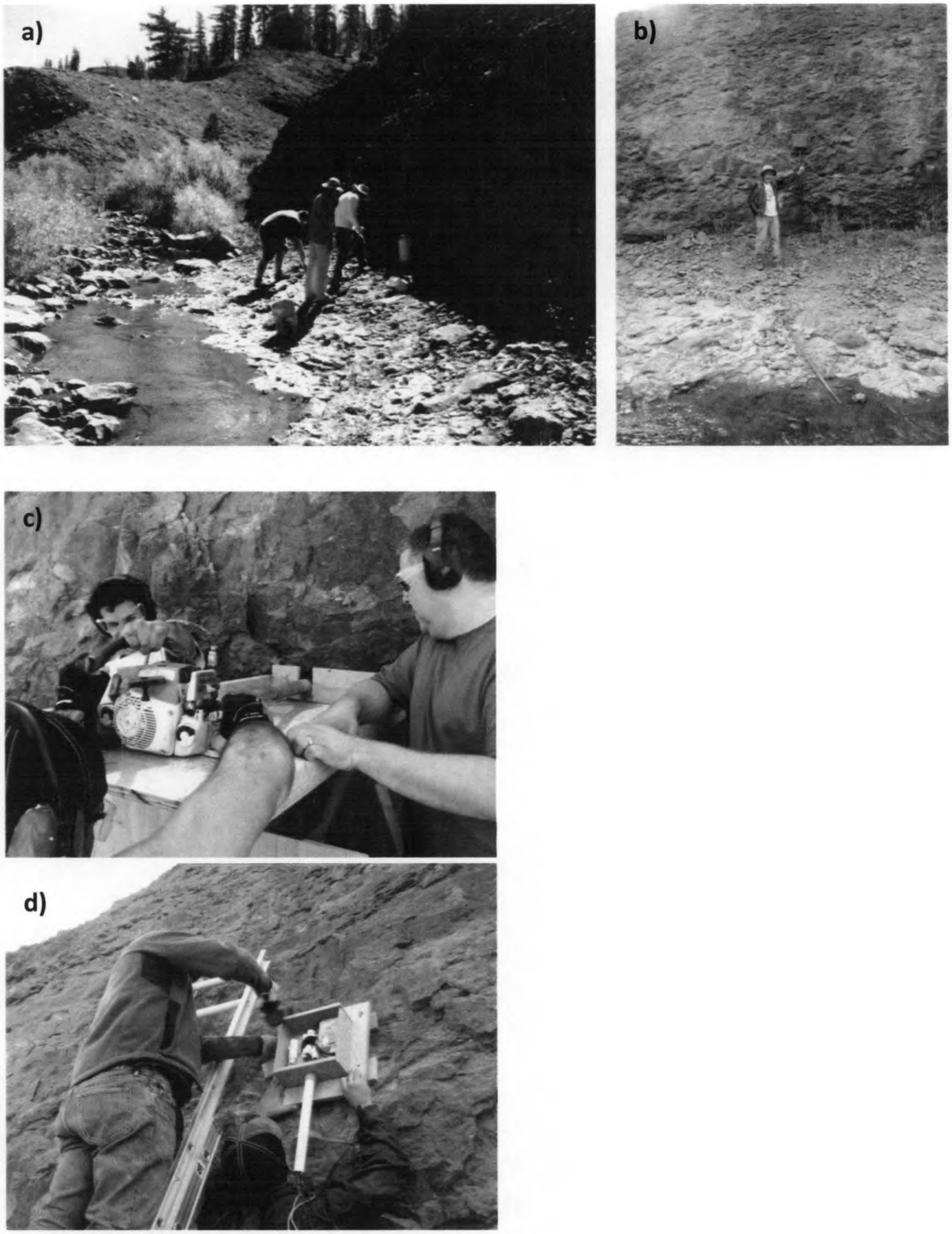

Figure 13. The NFM installation. **a)** Early stage site preparation. **b)** Completed installation. **c)** Drilling into cliff face. **d)** Electrical box for data loggers.

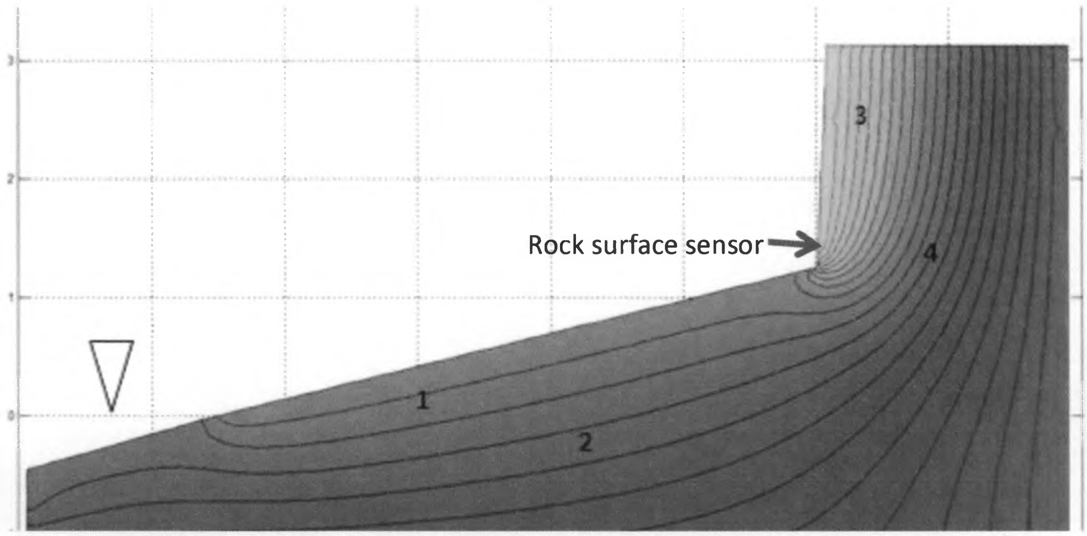

Figure 14. Cross-sectional view of the thermistor array. Grid line spacing is 1 m.

a)

b)

c)

d)

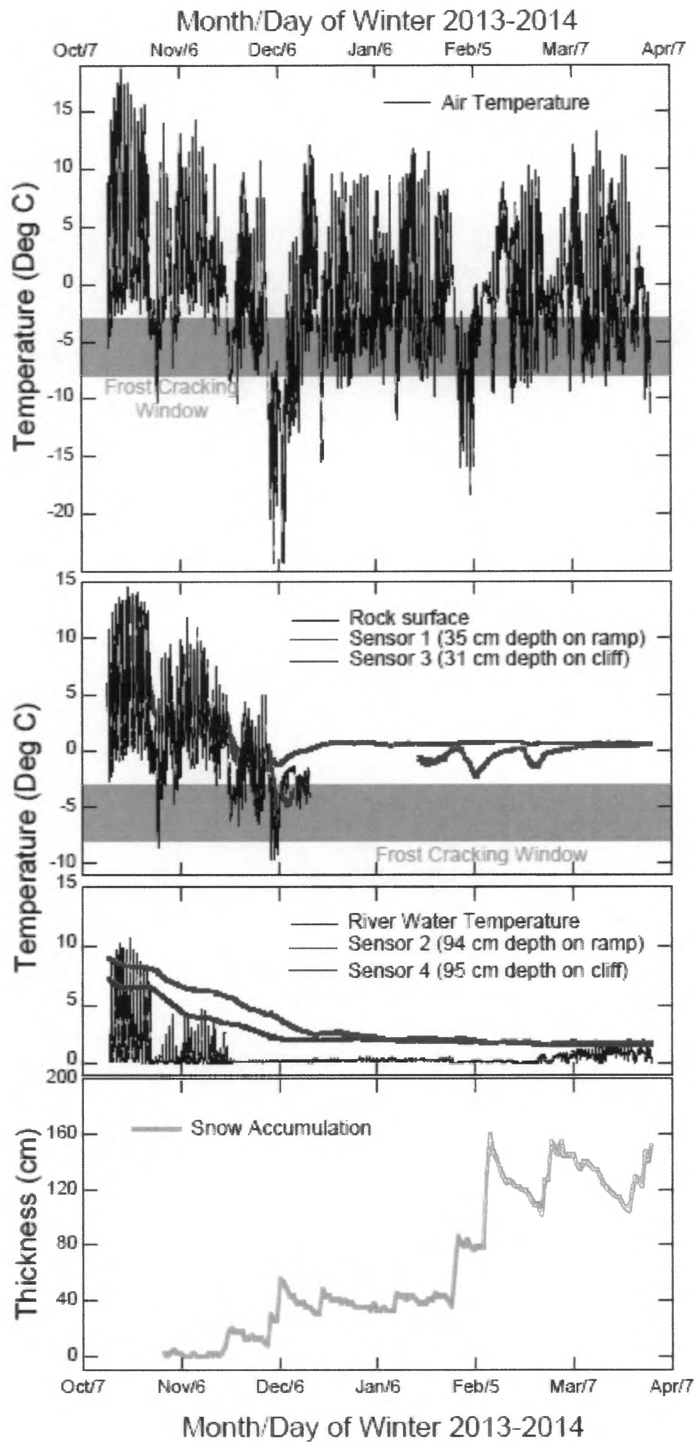

Figure 15. Temperature and snow record for winter 2013/2014. Sensor numbers correspond to those in **Figure 14**. **a)** Atmospheric temperature. **b)** Rock surface and sensors 1, 3. **c)** River temperature and sensors 2, 4. **d)** Snow depth record from Ebbetts Pass station, elevation 2670 masl, ~6 km from the NFM site. Elevation GAP in record for sensor 3 and the rock surface temperature attributable to logger malfunction.

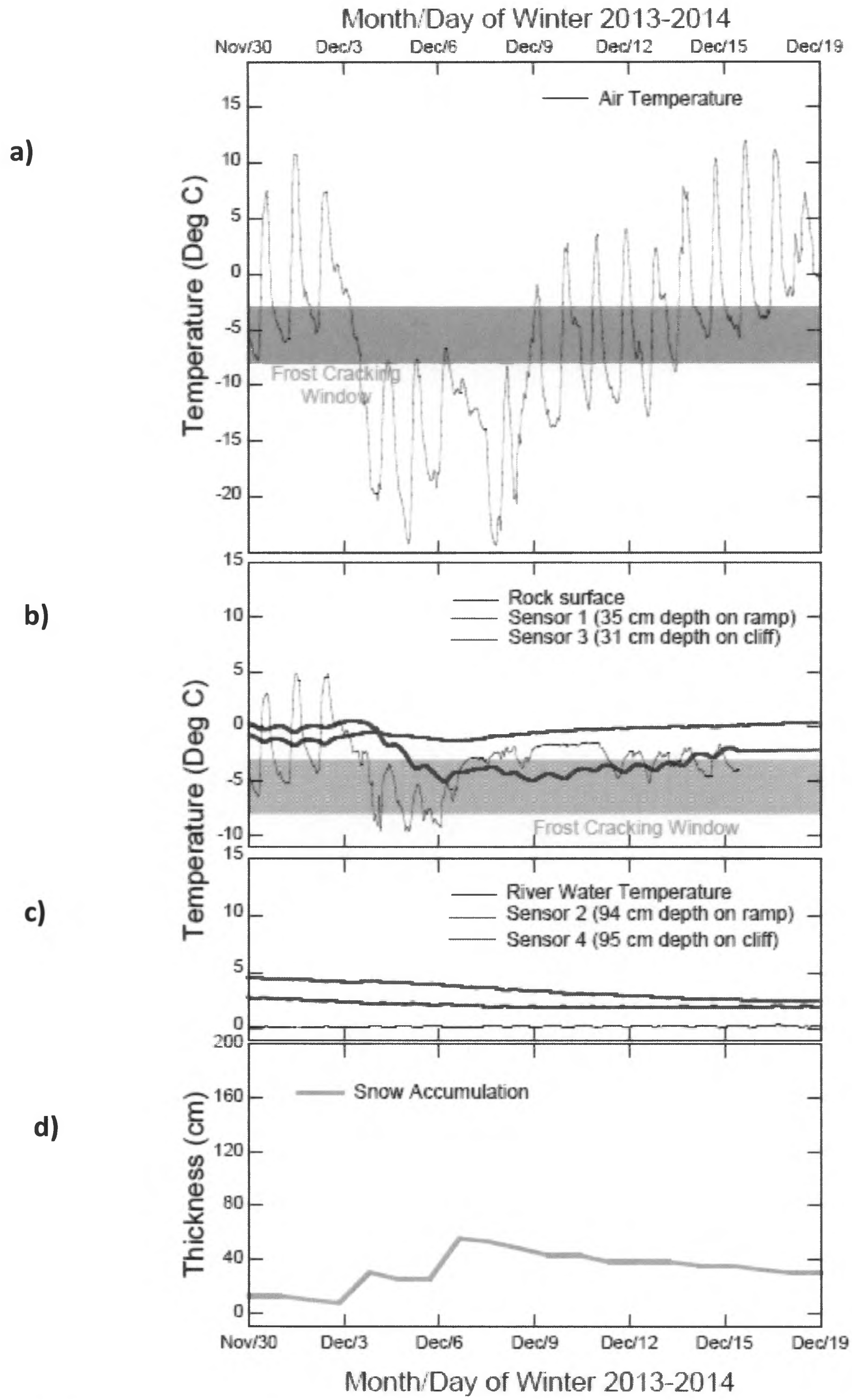

Figure 16. Temperature and snow detail of the December 2013 cold period. Record of rock surface temperature ends on December 16, due to data logger malfunction. . **a)** Atmospheric temperature. **b)** Rock surface and sensors 1, 3. **c)** River temperature and sensors 2, 4. **d)** Snow depth record from Ebbetts Pass station, elevation 2670 masl, ~6 km from the NFM site. Gap in record for sensor 3 and the rock surface temperature attributable to logger malfunction.

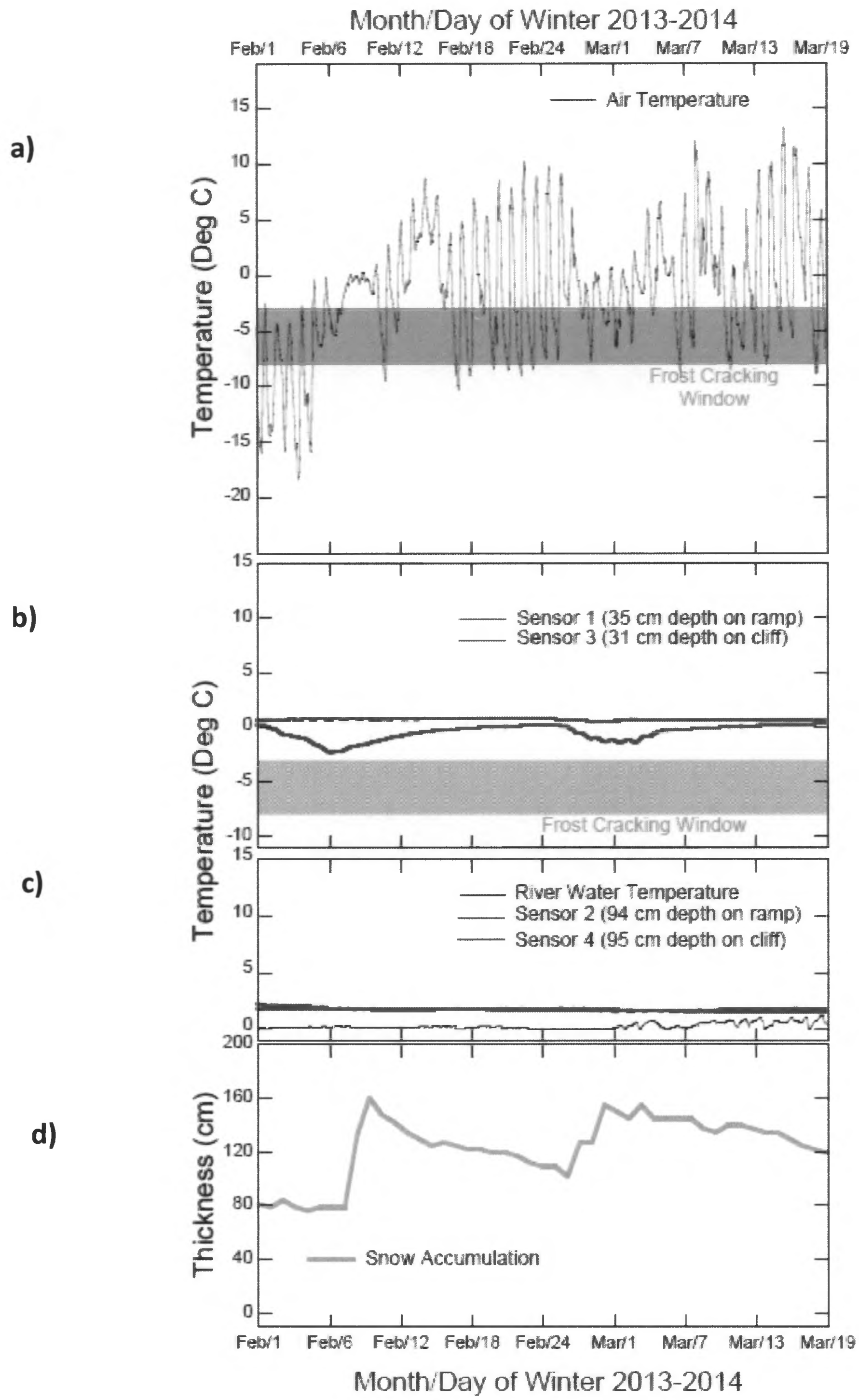

Figure 17. Temperature and snow detail of the February/March 2014 cold periods. Note the absence of a record for rock surface temperature due to data logger malfunction. . **a)** Atmospheric temperature. **b)** Sensors 1, 3. **c)** River temperature and sensors 2, 4. **d)** Snow depth record from Ebbetts Pass station, elevation 2670 masl, ~6 km from the NFM site. Elevation GAP in record for sensor 3 and the rock surface temperature attributable to logger malfunction.

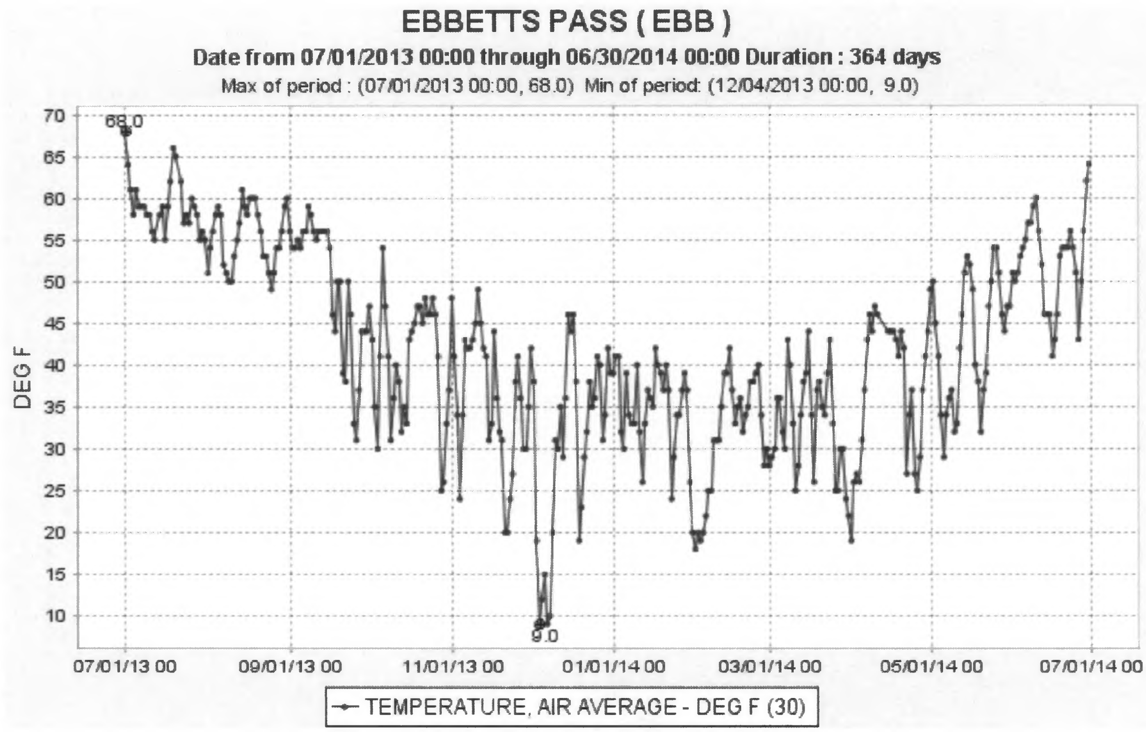

Figure 18. Temperature record for the twelve month period from the Ebbetts Pass station (Fig. 2). Average temperature for this period was 5.5 °C (41.9 °F).

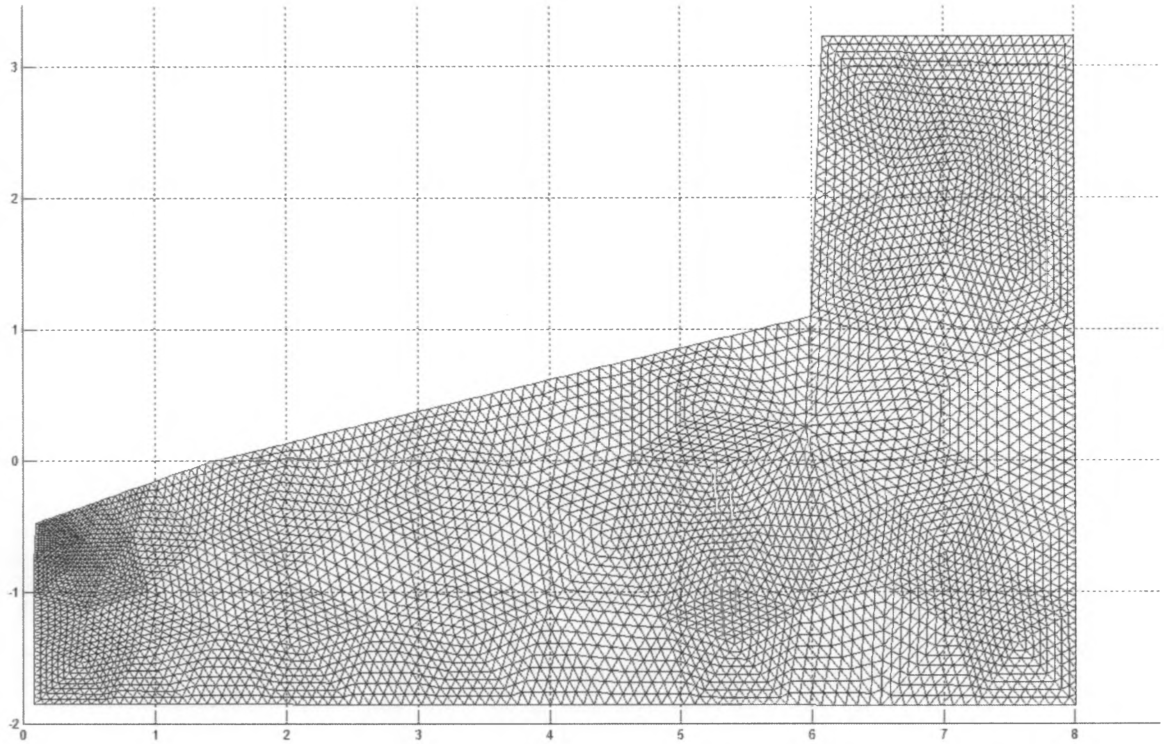

Figure 19. Sample finite element mesh used in 2D modeling. Mesh generated by Matlab PDEtoolbox. This mesh contains 4961 nodes and 9600 triangles.

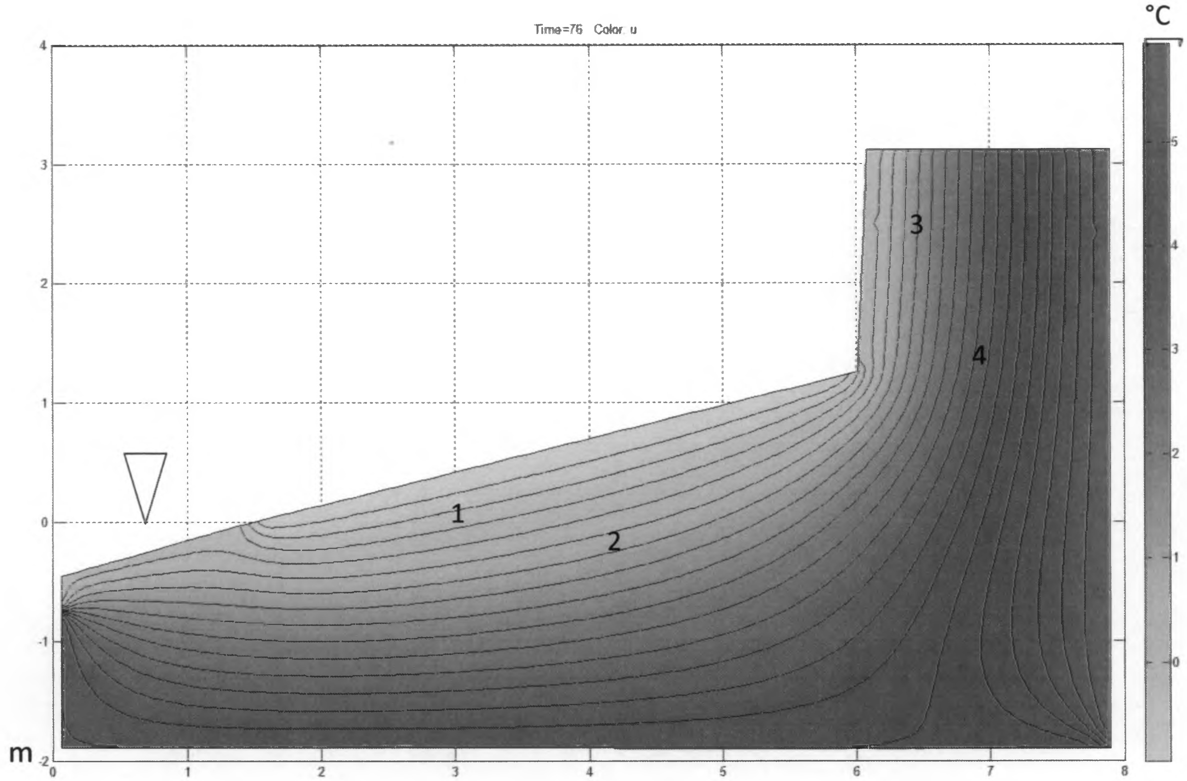

Figure 20. Model result for the first 24 hours ending 1800 on December 3. The grid is 1 m square and the scale conforms to the NFM study site. Inverted triangle denotes the low flow surface of the river. Results of the model are broadly consistent with the data on rock temperature (Table III). Isotherm contour interval is 0.35 °C. Numbers mark approximate locations of the sensors in the rock mass. Boundary conditions in the model: rock surface covered by the river, T = 0.14 °C; ramp surface, T = -1.02 °C; cliff surface T = 0.0 °C; right boundary of model space, T = 6.0 °C; lower boundary T = 4.0 °C.

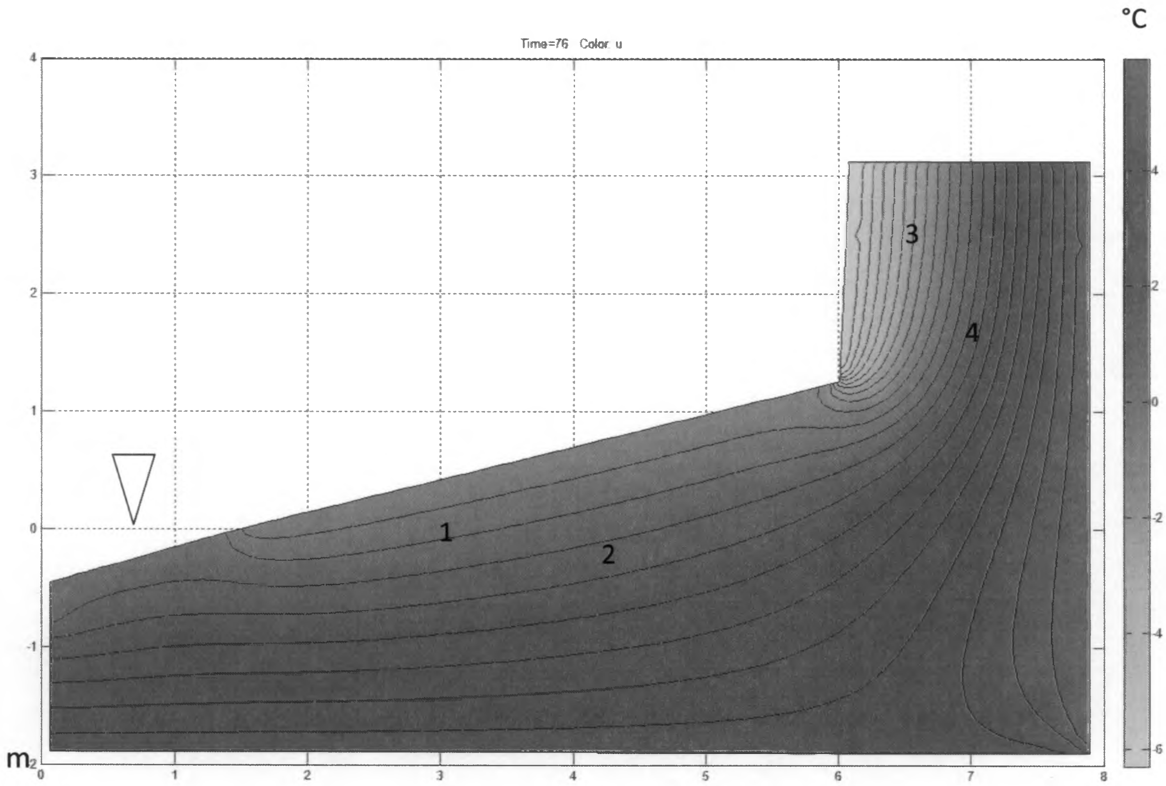

Figure 21. Model state at the end of the 76 hour period ending on December 6 at 2200. Note that the temperature scale differs from that in Figure 20. In this figure, the isotherm contour interval is 0.6 °C. The inverted triangle marks the low flow surface of the water. Numbers in plot mark the approximate positions of the sensors. Boundary conditions in the model: rock surface covered by the river, T = 0.20 °C; ramp surface, T = -1.0 °C; cliff surface, T= -6.5 °C; right boundary T= 6.0 °C; and lower boundary, T = 4.0 °C.

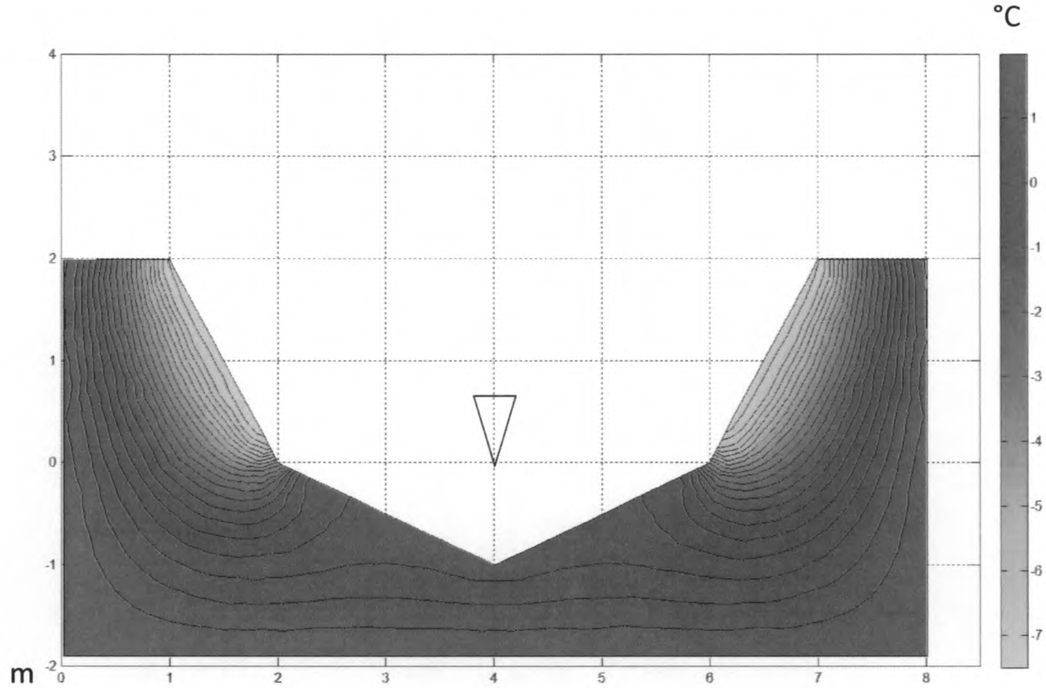

Figure 22. Modeled cross section of a river channel, using similar boundary conditions to those in the December 2013 cold period at the NFM study site. No snow cover is assumed in this variation.

Appendix A

Statistical analysis for determining *MAT* by elevation

Individual basin linear regressions:

Bivariate Fit of MAT (deg. C) By Elevation (m) Basin=Mokelumne

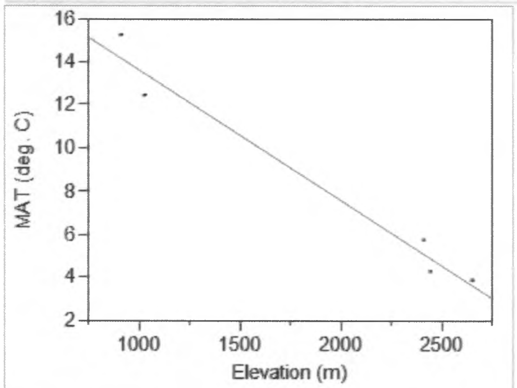

Linear Fit

Linear Fit

MAT (deg. C) = 19.704201 - 0.0060551*Elevation (m)

Summary of Fit

RSquare	0.972563
RSquare Adj	0.963418
Root Mean Square Error	0.994621
Mean of Response	8.288
Observations (or Sum Wgts)	5

Analysis of Variance

Source	DF	Sum of Squares	Mean Square	F Ratio
Model	1	105.20087	105.201	106.3419
Error	3	2.96781	0.989	Prob > F
C. Total	4	108.16868		0.0019*

Parameter Estimates

Term	Estimate	Std Error	t Ratio	Prob>|t|
Intercept	19.704201	1.193074	16.52	0.0005*
Elevation (m)	-0.006055	0.000587	-10.31	0.0019*

Bivariate Fit of MAT (deg. C) By Elevation (m) Basin=Stanislaus

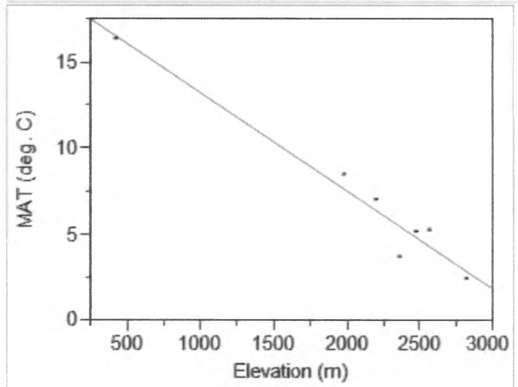

Linear Fit

Linear Fit

MAT (deg. C) = 18.949912 - 0.0056939*Elevation (m)

Summary of Fit

RSquare	0.958427
RSquare Adj	0.950113
Root Mean Square Error	1.027449
Mean of Response	6.9
Observations (or Sum Wgts)	7

Analysis of Variance

Source	DF	Sum of Squares	Mean Square	F Ratio
Model	1	121.68654	121.687	115.2715
Error	5	5.27826	1.056	Prob > F
C. Total	6	126.96480		0.0001*

Parameter Estimates

Term	Estimate	Std Error	t Ratio	Prob>|t|
Intercept	18.949912	1.187622	15.96	<.0001*
Elevation (m)	-0.005694	0.00053	-10.74	0.0001*

Bivariate Fit of MAT (deg. C) By Elevation (m) Basin=Tuolumne

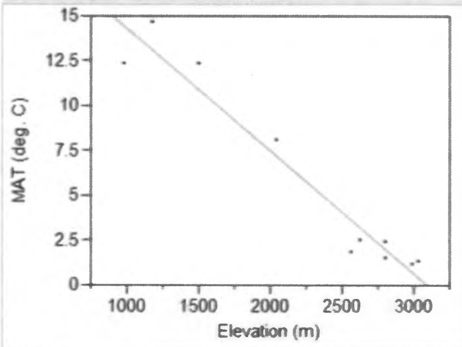

— Linear Fit

Linear Fit

MAT (deg. C) = 21.183989 - 0.0068302*Elevation (m)

Summary of Fit

RSquare	0.943819
RSquare Adj	0.936797
Root Mean Square Error	1.367521
Mean of Response	5.816
Observations (or Sum Wgts)	10

Lack Of Fit

Analysis of Variance

Source	DF	Sum of Squares	Mean Square	F Ratio
Model	1	251.33833	251.338	134.3974
Error	8	14.96091	1.870	Prob > F
C. Total	9	266.29924		<.0001*

Parameter Estimates

Term	Estimate	Std Error	t Ratio	Prob>|t|
Intercept	21.183989	1.394382	15.19	<.0001*
Elevation (m)	-0.00683	0.000589	-11.59	<.0001*

Bivariate Fit of MAT (deg. C) By Elevation (m) Basin=Merced

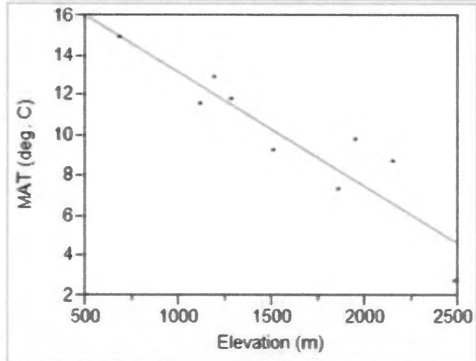

— Linear Fit

Linear Fit

MAT (deg. C) = 18.884489 - 0.0057099*Elevation (m)

Summary of Fit

RSquare	0.843327
RSquare Adj	0.820946
Root Mean Square Error	1.504768
Mean of Response	9.862222
Observations (or Sum Wgts)	9

Analysis of Variance

Source	DF	Sum of Squares	Mean Square	F Ratio
Model	1	85.31788	85.3179	37.6792
Error	7	15.85028	2.2643	Prob > F
C. Total	8	101.16816		0.0005*

Parameter Estimates

Term	Estimate	Std Error	t Ratio	Prob>|t|
Intercept	18.884489	1.553052	12.16	<.0001*
Elevation (m)	-0.00571	0.00093	-6.14	0.0005*

Summary of regression parameters:

Basin	Basin #	Slope	Std error	n	Intercept	Std error
Mokelumne	1	0.0061	0.000587	5	19.704	1.193
Stanislaus	2	0.0057	0.00053	7	18.95	1.188
Tuolumne	3	0.0068	0.000589	10	21.184	1.394
Merced	4	0.0057	0.00093	9	18.885	1.553

Experimentwise error:

α=0.05 K = 6

$\alpha_\epsilon=1-(1-\alpha)^k=$ 0.2649081

Pairwise t tests:

Comparison	Slope: d	S_d	t_{data}	$t_{0.05(2),v}$		Intercept: d	S_d	t_{data}	$t_{0.05(2),v}$
1X2	0.0004	0.000791	0.51	2.23		0.754	1.683625	0.45	2.23
1X3	0.0007	0.000832	0.84	2.16		1.48	1.834798	0.81	2.16
1X4	0.0004	0.0011	0.36	2.18		0.819	1.95833	0.42	2.18
2X3	0.0011	0.000792	1.39	2.13		2.234	1.831551	1.22	2.13
2X4	0	0.00107	0	2.14		0.065	1.955288	0.03	2.14
3X4	0.0011	0.001101	1.0	2.11		2.299	2.086874	1.10	2.11

The value of t_{data} is less than that of $t_{0.05(2),v}$ in each case. None of the differences in slope or intercept are statistically significant. Moreover, the experimentwise error would require a confidence level higher than 0.05 in order for any differences to be statistically significant. Hence, the region wide regression in equation (2) (Fig. 2) is used in the *MAT* by elevation plots and model solutions.

Appendix B

Geologic Setting of the Tuolumne Study Site

The study site on the Tuolumne River was selected because of its excellent bedrock exposures in the Tuolumne Intrusive Suite ("TIS") and its elevation of ~2620 masl at the margin of the meadow, descending to ~2440 masl at Glen Aulin. This elevation range places the Tuolumne study site in the frost cracking window (Fig. 1). The TIS is a concentric zoned plutonic sequence in the eastern portion of Yosemite National Park of mid to late Cretaceous age. The members of the TIS become progressively younger and more felsic, moving from the margin towards the center of the pluton (Bateman and Chappell, 1979). The units near the margin contain magmatic foliations striking subparallel to the margin of the suite (Fig. 9). The downstream sequence in the study area is Cathedral Peak Granodiorite ("Kcp"), the equiangular facies of the Half Dome Granodiorite ("Khd"), and the Tonalite of Glen Aulin ("Kga"). Kcp is a medium-grained hornblend-biotite granodiorite with conspicuous K-feldspar megacrysts, increasing in size towards the margin (up to 6-8 cm across). Magmatic foliation is sparse in Kcp (Bateman and Chappell, 1979). Kcp is crosscut by leucocratic dikes (apatite and pegmatite). Khd is a medium-grained granodiorite characterized by euhedral hornblend prisms, 1 cm biotite crystals, and conspicuous sphene. Khd contains steeply dipping to vertical magmatic foliations, striking northeast (~normal to the trend of the river along the traverse). Kga is a fine-grained, dark quartz diorite along the traverse. The magmatic foliation is similar in strike and dip to that in Khd.

Contained within Kcp on the left bank of the Tuolumne River is the Little Devils Postpile ("LDP"). LDP is a volcanic plug of trachyandesite (Glazner and Stock, 2010) of Miocene age. The outcrop is mapped as Ttb (Fig. 9). LDP is composed of horizontally oriented columnar joints. Because columnar joints are oriented normal to the coolest contact (Degraff and Aydin, 1987), the horizontal orientation is evidence that the lava cooled in the subsurface in con*ta*ct with Kcp. The Kcp north bank of the river displays evidence of partial melting due to its dark color (quartz glass) and "splotchy" white feldspar crystals.

At the outer margin of the TIS, the Tuolumne River cuts through an aureole of pre-Cretaceous calc-silicate metasedimentary rock. This remnant of country rock would have experienced high rates of strain during the emplacements of the TIS and the older Hoffman Peak pluton ("Kh") on its western margin (Albertz et. al., 2005).

Appendix C

Anova Analysis of Kcp Joint Spacing

Oneway Analysis of Spacing(cm) By Bank/notBank

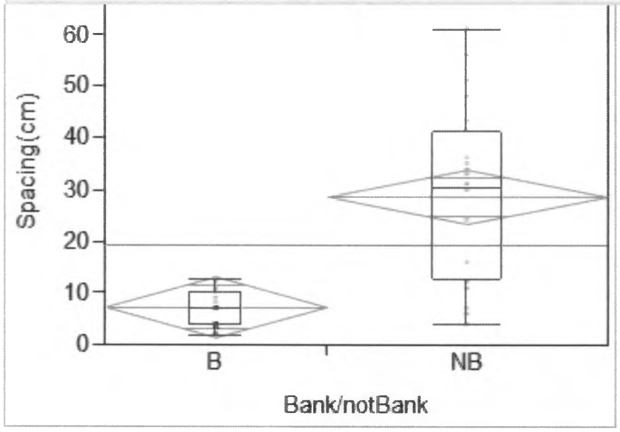

Quantiles

Level	Minimum	10%	25%	Median	75%	90%	Maximum
B	2	2	4	7	10	12	13
NB	4	6.5	13	30.5	41.25	53.5	61

Oneway Anova

Summary of Fit

Rsquare	0.422693
Adj Rsquare	0.408612
Root Mean Square Error	12.69656
Mean of Response	19.18605
Observations (or Sum Wgts)	43

t Test

NB-B

Assuming equal variances

Difference	21.3618	t Ratio	5.478994
Std Err Dif	3.8989	DF	41
Upper CL Dif	29.2358	Prob > |t|	<.0001*
Lower CL Dif	13.4879	Prob > t	<.0001*
Confidence	0.95	Prob < t	1.0000

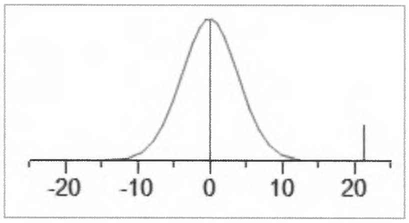

Appendix D

Thermal Diffusivity

Thermal diffusivity is a material property that is the ratio of thermal conductivity to density time's heat capacity. I derived a first order estimate of thermal diffusivity at the NFM site from the exponential term in equation (1). A formula for an attribute called skin depth (δ) is derived from this term.

$$\delta = z/\ln(A_0/A_z) \quad (4)$$

A_0 and A_z are, respectively, amplitude of the temperature fluctuation at the surface and at some specified depth. To calculate values for these variables I used data from the period October 15-26, 2013 during which the temperature ranges were relatively stable. Using the data from the rock surface sensor and sensor 1, A_0 = 6.92 °C and A_{35} = 0.53 °C and δ = 136 mm. Thermal diffusivity is calculated as follows:

$$\alpha = 0.5\delta^2\omega \quad (5)$$

For the selected period, the result is α = 0.68 mm^2s^{-1}. This result can only be regarded as a first order estimate because the diurnal fluctuations in temperature are not perfectly sinusoidal. However, the estimate falls within the range of values derived from laboratory experiments reported in the literature, 0.6 to 2.0 mm^2s^{-1} and is similar to a reported value of 0.69 mm2s-1 for basalt (Drury, 1987).

It has also been shown that thermal diffusivity increases with decreasing temperature in the material (Vosteen and Schellschmidt, 2003). Laboratory measurements of thermal diffusivity are typically conducted in ambient temperatures of ~20 °C. For magmatic rock, Vosteen and Schellschmidt (2003) showed thermal diffusivity increases by ~15% in moving from ~20 to 0 °C. For this study, thermal diffusivity at temperatures < 0 °C is of greatest interest. Hence, in both the 1D and 2D modeling, I use $\alpha = 1.0\ mm^2s^{-1}$.

Appendix E

Matlab PDE toolbox

The following screen shots illustrate the PDE toolbox methodology. The illustration demonstrates the development of Figure 21.

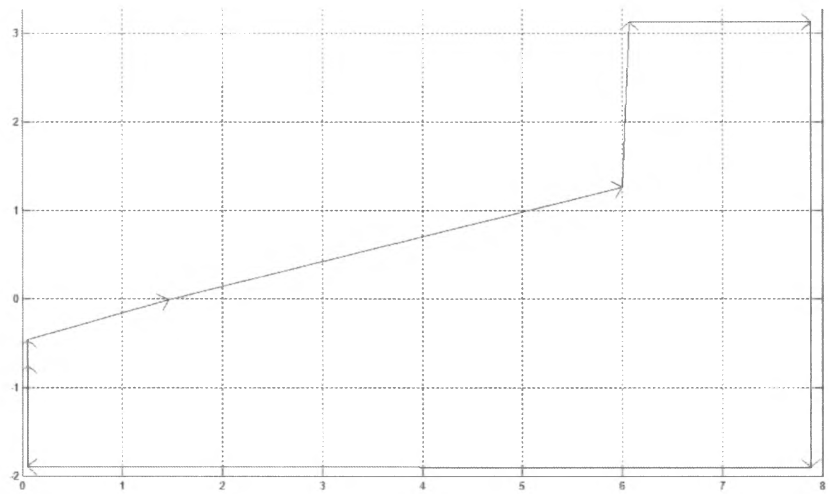

Step 1: Draw geometry of the model space. Each arrow represents a boundary for which an unique boundary condition may be specified. Blue arrows indicate von Neumann boundary conditions (based on first derivative). Red arrows indicate Dirichlet boundary conditions (based on fixed temperature).

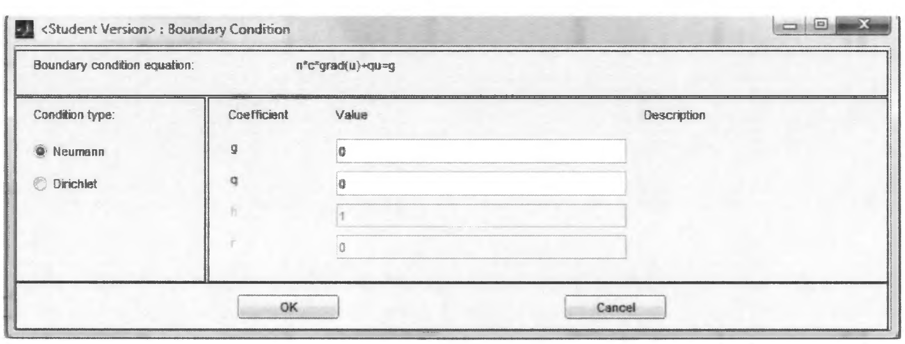

Step 2: Set von Neumann boundary conditions to T' = 0,

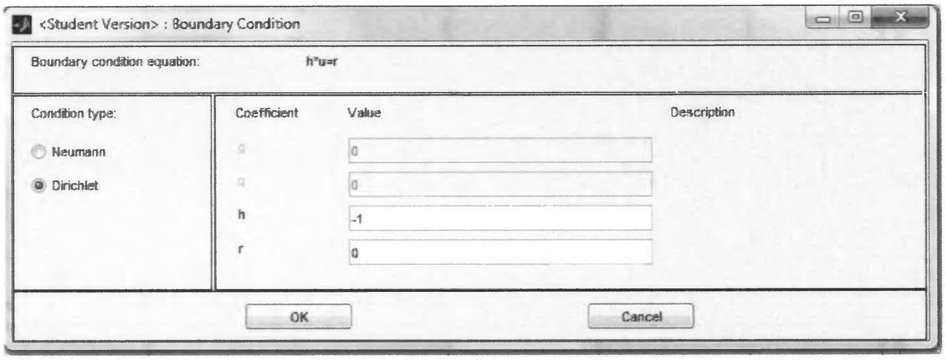

Step 3: Set Dirichlet boundary conditions. Illustrates ramp boundary T = -1.0.

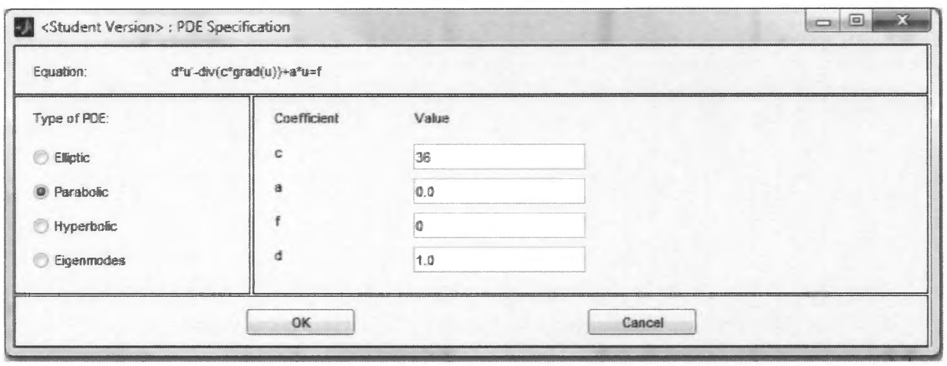

Step 4: Specify PDE. In case, a scalar parabolic PDE, the heat equation.

$c = \alpha = 36\ cm^2hr^{-1}$.

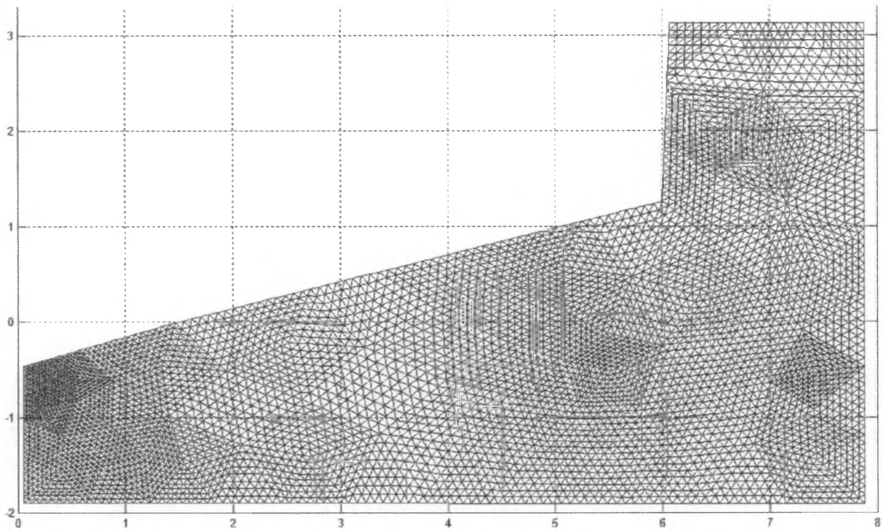

Step 5: Initiate finite element triangular mesh. This case is three refinements of the initial mesh with 4961 nodes and 9600 triangles.

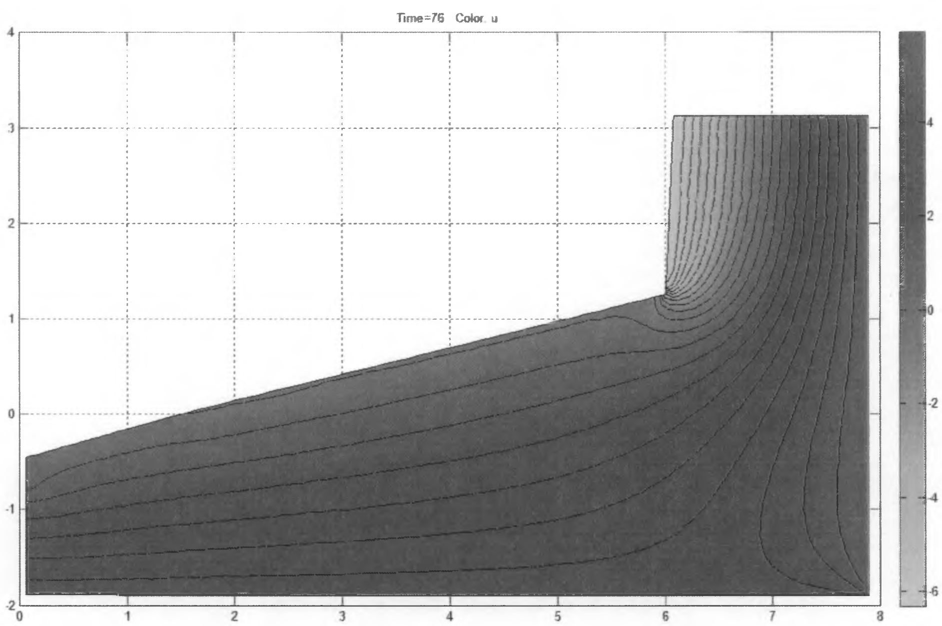

Step 6: Plot solution with 20 isotherms.